

Simulating biochemical reactions: The Linear Noise Approximation can capture non-linear dynamics

Frederick Truman-Williams^a and Giorgos Minas^{b,1}

^a*Mathematical Institute, University of Oxford, Oxford, OX2 6GG, United Kingdom*

^b*School of Mathematics and Statistics, University of St Andrews, St Andrews, KY16 9SS, Scotland, United Kingdom**

Abstract

There is a plethora of highly stochastic non-linear dynamical systems in fields such as molecular biology, chemistry, epidemiology, and ecology. Yet, none of the currently available stochastic models are both accurate and computationally efficient for long-term predictions of large systems. The Linear Noise Approximation (LNA) model for biochemical reaction networks is analytically tractable, which makes it computationally efficient for simulation, analysis, and inference. However, it is only accurate for linear systems and short-time transitions. Other methods can achieve greater accuracy across a wider range of systems, including non-linear ones, but lack analytical tractability. This paper seeks to challenge the prevailing view by demonstrating that the Linear Noise Approximation can indeed capture non-linear dynamics after certain modifications. We introduce a new framework that utilises centre manifold theory allowing us to identify simple interventions to the LNA that do not significantly compromise its computational efficiency. We develop specific algorithms for systems that exhibit oscillations or bi-stability and demonstrate their accuracy and computational efficiency across multiple examples.

Throughout biology, ecology, epidemiology and other fields, there is a plethora of non-linear dynamical phenomena such as oscillations and multi-stabilities. Examples include the circadian rhythms [21], embryonic development oscillations [39], cell signalling oscillations [4], multi-stabilities in cell cycle [45, 46, 2], cell differentiation [8, 19], and apoptosis [3], the central carbon metabolism in *E.coli* [26], predator-prey oscillations in ecology [11], and epidemic oscillations [62]. These non-linear dynamics are caused by feed-forward loops [38], negative feedback loops [38, 48] and other mechanisms, which are operated by networks of interacting species. For example, gene expression oscillations are often generated when a gene directly suppresses its own expression or activates the expression of its suppressors. In infectious diseases outbreaks, compartments of the population, such as infected and recovered individuals, interact between each other and phenomena like awareness and fatigue can generate oscillatory behaviors [62]. The effects of stochasticity in these interactions, caused by molecular diffusion or, more generally, the complex environment in which these interactions occur, are significant, especially when dealing with smaller populations. Yet modeling the stochasticity using fast, accurate, scalable methods is an unsolved problem.

These networks of stochastic interactions are often called reaction networks. The term reaction is not only used for biochemical reactions but any event that directly causes a change in the population of one or more species. The stochastic dynamics of reaction networks, can be described, under certain assumptions, by Markov processes $\{\mathbf{Y}(t) = (Y_1(t), \dots, Y_n(t))^T \mid t \geq 0\}$, describing the evolution of n populations of different species over time. The so-called (chemical) master equation [13], which describes

*To whom correspondence should be addressed. E-mail: gm256@st-andrews.ac.uk

the evolution of the probability distribution of the species populations, can be solved only rarely, severely limiting its tractability. The stochastic simulation algorithm (SSA) [14] produces exact simulations of the master equation but it is far too slow to be used in most applied settings since it simulates every single reaction event.

At present, there are many methods of approximation of the master equation that target accelerating simulation. Examples include tau leaping algorithms [17, 18] and the numerical integration of the (chemical) Langevin equations [16]. Both rapidly increase the speed of simulation, however they leave no scope for studying the distributions of the reaction network’s species analytically, and can be extremely slow for sensitivity analysis and parameter estimation. Other recent methods [6, 28] focus on approximating any protein-binding reactions, that often appearing in molecular biology networks, with simpler, analytically tractable reactions.

Much work has followed from van Kampen’s system size expansion [58], which uses a system size parameter Ω (like cell volume in molecular biology, population size in ecology or epidemiology) to derive approximations of the master equation. Under certain conditions, the deterministic process $\{\mathbf{x}(t) \mid t \geq 0\}$ which solves the macroscopic reaction-rate equations was shown to be the limit, as $\Omega \rightarrow \infty$, of the solutions of the master equation [32, 33]. The Linear Noise Approximation (LNA), derived using the system size expansion, is a stochastic model that provides even more rapid simulation than the aforementioned stochastic methods as well as being the only model in this field that allows analytical expressions of probability distributions of the state of the system at arbitrary time-points. This makes the LNA a powerful tool for sensitivity analysis and statistical inference [41, 42, 54, 43, 31, 10, 20, 49].

However, the important drawback of using the LNA is its inability to approximate the long-term behavior of reaction networks exhibiting non-linear dynamics. Indeed, when the system dynamics are non-linear [61], predictions of the state of the system at time t given the state at an earlier time s become inaccurate as $t - s$ becomes large. For a given reaction network, we can qualitatively examine the dynamics of its paths and identify different phases of their evolution - for instance peaks and troughs in species populations. If we were to examine the distribution of entire stochastic paths generated by the SSA in a finite number of time-points then we find that, the phases of such paths become out of sync with what the LNA predicts their phases to be. Hence the LNA makes incorrect predictions of the dynamics thereafter. In [41], it was shown that in the specific setting where the macroscopic ($\Omega \rightarrow \infty$) deterministic approximation has an attractive limit cycle solution, correcting these drifts in phase predicted by the LNA is sufficient to produce simulations that are nearly identical to those produced by the SSA. This approach enables the construction of both fast and accurate algorithms for stochastic simulation, sensitivity analysis, and statistical inference of this class of non-linear systems [41].

There are three fundamental results in this paper. Firstly, we show that the analytically tractable LNA model, which is known to be long-time accurate only for linear systems, can also be applied to non-linear systems after appropriate modifications. In particular, we illustrate that it *can* accurately describe long-term stochastic dynamics for arguably the two most abundant non-linear phenomena: oscillations and bi-stability. We demonstrate this on several systems including the oscillatory systems in [35, 63, 4], and bi-stable systems in [12, 2, 19]. Secondly, as part of this effort, we build a new framework for constructing LNA-based models for non-linear dynamical systems. We call the models developed using our framework phase corrected LNA (pcLNA) models because they use the LNA model equations to evolve the system except that the phase of the system is adjusted in frequent times to control phase drifts. Fundamental to the pcLNA approach is a mapping G that computes the phase of any stochastic state allowing for any phase drift to be corrected. We show that for the very large class of systems whose macroscopic reaction rate equation exhibits a non-hyperbolic equilibrium, the theory of centre manifolds of dynamical systems can be employed to explicitly define the phase correction map G . Thirdly, we illustrate *how* the pcLNA framework can be applied to accurately describe reaction networks whose macroscopic deterministic evolution $\{\mathbf{x}(t) \mid t \geq 0\}$ exhibits Hopf bifurcation and those exhibiting bi-stability in a region of their parameter space. That is, systems with oscillations; sustained or non-sustained and often determined by only a small change in a parameter, or systems which can switch between two steady states due to

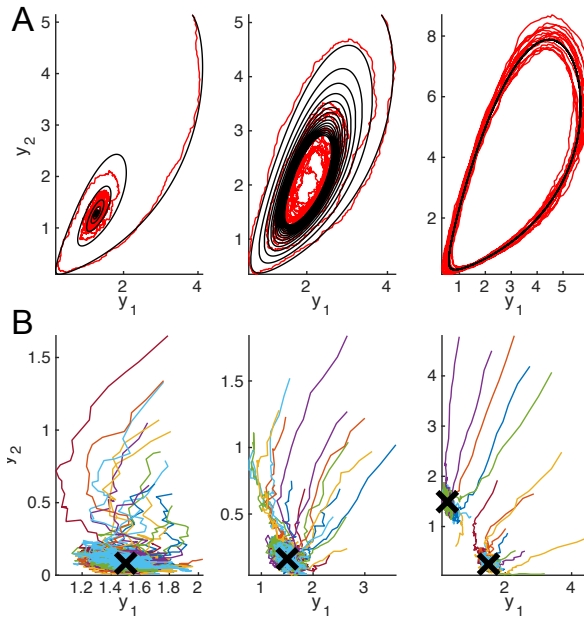


Figure 1: A. Phase portraits of RRE solutions in (6) and a SSA simulation (red) for the system in [63]. B. Phase portraits of 20 SSA simulations (color) and the fixed points of the RRE in (6) (crosses) for the system in [12]. The qualitative changes from left to right figure are due to changes in the bifurcation parameter value.

stochasticity. We demonstrate that the pcLNA model for these systems offers accurate approximations of the master equation for long-term simulation whilst substantially reducing the simulation time by several orders of magnitude. Perhaps even more importantly, the accuracy of the pcLNA models opens up the possibility of using its tractability to perform computationally demanding tasks such as sensitivity analysis, inference and prediction.

While the approach developed in [41] demonstrated that phase correction significantly improves the long-term accuracy of the LNA in oscillatory systems with stable limit cycles, it was limited to this specific dynamical setting. In contrast, the framework introduced in this paper generalises the concept of phase correction by introducing centre manifold theory to define and correct phase drifts in a broader class of systems—specifically, those with non-hyperbolic equilibria, including both oscillatory and bi-stable dynamics. This theoretical foundation enables us to construct a unified, algorithmic approach for defining and correcting phase across diverse nonlinear regimes, allowing the pcLNA to extend the analytical tractability and computational efficiency of the LNA to a significantly wider class of biologically relevant systems.

We begin in Section 1 by introducing the pcLNA modelling framework. We first review reaction networks and the system size expansion in Sections 1.1 and 1.2, before introducing the Linear Noise Approximation (LNA) in Section 1.3. We then discuss the LNA’s loss of accuracy in non-linear systems and introduce the concept of phase in this context. In Section 1.4, we present the phase corrected LNA (pcLNA), followed by the theoretical foundation of our approach—centre manifold theory—in Section 1.5, with further implications discussed in Section 1.6. In Section 2, we apply our framework to reaction networks whose macroscopic reaction rate equation undergoes a Hopf bifurcation and develop the pcLNA algorithm specific to these systems. Section 3 focuses on bi-stable systems and constructs the corresponding pcLNA algorithms. We validate our framework through numerical investigations in

Section 4, and conclude with a discussion of our findings and future directions in Section 5. Additional numerical investigations demonstrating the accuracy of the pcLNA modelling techniques on other reaction networks, as well as supporting technical results and derivations, are provided in the Supporting Information (SI).

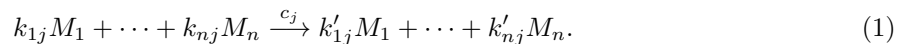
Results

1 The pcLNA modelling framework

1.1 Reaction networks

We begin by presenting a mathematical formulation of reaction networks. We describe this framework within the context of molecular biology, although analogous terminology can be applied in other fields such as epidemiology and ecology (see, for instance, [20, 64]).

A system of multiple different molecular sub-populations, M_1, M_2, \dots, M_n has state vector, $\mathbf{Y}(t) = (Y_1(t), \dots, Y_n(t))^T$ where $Y_i(t) \geq 0$, $i \in \{1, \dots, n\}$, denotes the number of M_i molecules at time t . These molecules undergo reactions R_j , $j \in \{1, \dots, r\}$, such as transcription, translation, degradation and translocation, which change the number of molecules of each specie,



Here, the non-negative coefficients $k_{ij}, k'_{ij} \geq 0$ denote the number of molecules of M_i involved as reactants and products, respectively, in reaction R_j . If R_j occurs at time $t \geq 0$, $\mathbf{Y}(t)$ jumps to a new state $\mathbf{Y}(t) + \boldsymbol{\nu}_j$, where the transition vectors $\boldsymbol{\nu}_j = (k'_{1j} - k_{1j}, \dots, k'_{nj} - k_{nj})^T \in \mathbb{R}^n$ are often called stoichiometric. Under the assumption that these reactions occur in a well-mixed solution [14], we can derive the propensity functions $\pi_j : \mathbb{R}^n \rightarrow [0, \infty)$ for each $j \in \{1, \dots, r\}$ with the probability of one R_j reaction occurring in the next infinitesimal time interval $[t, t + dt)$

$$P(\mathbf{Y}(t + dt) - \mathbf{Y}(t) = \boldsymbol{\nu}_j) = \pi_j(\mathbf{Y}(t))dt + o(dt^2). \quad (2)$$

The propensity functions π_j along with the stoichiometric vector $\boldsymbol{\nu}_j$, $j = 1, \dots, r$ completely specify the evolution of the reaction network.

The general form of the propensity function of the reaction in (1) is $\pi_j(\mathbf{y}) = c_j \prod_i y_i^{k_{ij}}$, with uni-molecular ($M_i \xrightarrow{c_j} \cdot$) and bi-molecular reactions ($M_i + M_{i'} \xrightarrow{c_j} \cdot$) with propensity of the form $c_j y_i$ and $c_j y_i y_{i'}$, respectively, being the most common type [60]. Here $c_j \in \mathbb{R}$ is the reaction rate constant corresponding to reaction R_j . The propensity functions are not restricted to the above general form. For instance, for enzymatic reactions involving species M_i the propensity has the Michaelis-Menten form [29], $c_2 y_i / (c_1 + y_i)$, while the Hill form [24], $c_2 y_i^h / (c_1^h + y_i^h)$, is also often used to reflect cooperative binding. For a discussion on the latter forms of propensities see [6].

These conditions give rise to a time-inhomogeneous, discrete state-space Markov process $\{Y(t) \mid t \geq 0\}$. The Kolmogorov forward equation [15] describing the evolution of the probability distribution, $P(\mathbf{y}, t) := P(\mathbf{Y}(t) = \mathbf{y} \mid \mathbf{Y}(t_0) = \mathbf{y}_0)$, of the stochastic process $\{\mathbf{Y}(t) \mid t \geq 0\}$ is,

$$\frac{\partial P(\mathbf{y}, t)}{\partial t} = \sum_{j=1}^r \pi_j(\mathbf{y} - \boldsymbol{\nu}_j) P(\mathbf{y} - \boldsymbol{\nu}_j, t) - \sum_{j=1}^r \pi_j(\mathbf{y}) P(\mathbf{y}, t). \quad (3)$$

The Kolmogorov equation is often referred as (chemical) master equation. Despite the equation only being analytically tractable for few cases, an exact simulation algorithm is available, namely Gillespie's stochastic simulation algorithm (SSA) [14]. We provide details of this in SI (Section S1).

1.2 System Size Expansion

The time-evolution of the stochastic process $\{\mathbf{Y}(t) \mid t \geq 0\}$ can be described using the random time change representation (RTC) [1]

$$\mathbf{Y}(t) = \mathbf{Y}(0) + \sum_{j=1}^r \nu_j N_j \left(\int_0^t \pi_j(\mathbf{Y}(s)) ds \right), \quad (4)$$

where, for $j \in \{1, \dots, r\}$, N_j are independent, unit Poisson processes corresponding to reaction R_j . This implies that for a given trajectory $\mathbf{Y}(s)$, $s \in [0, t)$, the random variables $N_j \left(\int_0^t \pi_j(\mathbf{Y}(s)) ds \right)$ are independent and have Poisson distribution with mean $\int_0^t \pi_j(\mathbf{Y}(s)) ds$.

In pursuit of seeking methods to approximate the process $\{\mathbf{Y}(t) \mid t \geq 0\}$, it is common to introduce a system size parameter Ω . Through setting $\mathbf{X}(t) := \mathbf{Y}(t)/\Omega$, one can study the dependence of stochastic fluctuations upon system size. It is sufficient to assume that the rates $\pi_j(\mathbf{Y}(t))$ depend upon Ω as $\pi_j(\mathbf{Y}(t)) := \Omega \rho_j(\mathbf{Y}(t)/\Omega)$ where ρ_j are called macroscopic rates of the system. This is a fairly-relaxed condition, that can be further relaxed to more general relations between the two functions [58, 33].

Using this condition, we can re-write the infinitesimal RTC equation in (18) in terms of $\mathbf{X}(t)$ as

$$\mathbf{X}(t + dt) - \mathbf{X}(t) = \sum_{j=1}^r \nu_j \Omega^{-1} N_j (\Omega \rho_j(\mathbf{X}(t)) dt), \quad (5)$$

with $\mathbf{X}(0) = \mathbf{X}_0$, thus providing a time evolution law for the process $\{\mathbf{X}(t) \mid t \geq 0\}$. If, for each $t \geq 0$, we define $\mathbf{x}(t)$ as the limit in probability of $\mathbf{X}(t)$ as $\Omega \rightarrow \infty$, we can use the law of large numbers¹ (see [32, 33]) to derive the limit of equation (5), as $\Omega \rightarrow \infty$, $\mathbf{x}(t + dt) - \mathbf{x}(t) = \sum_{j=1}^r \nu_j \rho_j(\mathbf{x}(t)) dt$, $\mathbf{x}(0) = \mathbf{x}_0$. Letting $dt \rightarrow 0$ we derive the macroscopic reaction rate equation (RRE), corresponding to the classical mass-action kinetics. Typical in applied biochemical settings is the need to study the qualitative changes in the dynamics of $\{\mathbf{X}(t) \mid t \geq 0\}$ and $\{\mathbf{x}(t) \mid t \geq 0\}$ when one (or more) of the system parameters, say α , is free to vary. To emphasize this dependence on parameter $\alpha \in \mathbb{R}$ we write the RRE as

$$\dot{\mathbf{x}} = \mathbf{F}(\mathbf{x}, \alpha), \quad \mathbf{F}(\mathbf{x}, \alpha) = \sum_{j=1}^r \nu_j \rho_j(\mathbf{x}(t), \alpha), \quad \mathbf{x}(0) = \mathbf{x}_0. \quad (6)$$

and the corresponding Jacobian matrix

$$\mathbf{J} = \mathbf{J}(\mathbf{x}, \alpha) = (\partial F_i / \partial x_j)_{i,j=1}^n \quad (7)$$

We will refer to the parameter α as the bifurcation parameter.

1.3 The Linear Noise Approximation (LNA)

To take into account the stochasticity of molecular interactions, one approach is to define the LNA ansatz equation [58, 32, 33] that describes the relation between the stochastic process $\{\mathbf{X}(t) \mid t \geq 0\}$ and the deterministic process $\{\mathbf{x}(t) \mid t \geq 0\}$. Their difference, scaled by $\Omega^{-1/2}$, is a stochastic process, $\{\boldsymbol{\xi}(t) \mid t \geq 0\}$, describing the noise around $\{\mathbf{x}(t) \mid t \geq 0\}$. That is, for each $t \geq 0$,

$$\mathbf{X}(t) = \mathbf{x}(t) + \Omega^{-1/2} \boldsymbol{\xi}(t). \quad (8)$$

¹Note that for a sequence X_1, X_2, \dots , of independent $\text{Poi}(\lambda)$ random variables ($0 < \lambda < \infty$), $N^{-1} \sum_{i=1}^N X_i$ converges in probability to λ , as $N \rightarrow \infty$.

As we show in SI (Section S2) by applying a derivation similar to [1] we get that for sufficiently large values of Ω , the time-evolution of $\{\boldsymbol{\xi}(t), t \geq 0\}$ can be described by the linear Stochastic Differential equation (in the Itô sense)

$$d\boldsymbol{\xi} = \mathbf{J}\boldsymbol{\xi}dt + \mathbf{E}d\mathbf{B}_t, \quad (9)$$

where \mathbf{J} is the Jacobian matrix in (7), $\mathbf{E} = \mathbf{E}(\mathbf{x}) = \mathbf{S}\text{diag}(\sqrt{\rho_1(\mathbf{x})}, \dots, \sqrt{\rho_r(\mathbf{x})})$ the product of the stoichiometry matrix $\mathbf{S} = [\boldsymbol{\nu}_1 \cdots \boldsymbol{\nu}_r]$, and the square root of the diagonal matrix, with main diagonal entries $(\rho_1(\mathbf{x}), \dots, \rho_r(\mathbf{x}))$, and \mathbf{B}_t an n -dimensional Wiener process.

This linear SDE in (25) has a solution that can be written as

$$\boldsymbol{\xi}(t) = \mathbf{C}(s, t)\boldsymbol{\xi}(s) + \boldsymbol{\eta}(s, t), \quad \boldsymbol{\eta}(s, t) \sim \text{MVN}(0, \mathbf{D}(s, t)), \quad (10)$$

where $\mathbf{C}(s, t)$ the fundamental matrix of (6), that is the solution of the initial value problem

$$\dot{\mathbf{C}} = \mathbf{J}\mathbf{C}, \quad \mathbf{C}(s, s) = \mathbf{I}, \quad (11)$$

and $\mathbf{D}(s, t)$ the symmetric, positive-definite matrix, which is a solution of the initial value problem

$$\dot{\mathbf{D}} = \mathbf{J}\mathbf{D} + \mathbf{D}\mathbf{J}^\top + \mathbf{E}\mathbf{E}^\top, \quad \mathbf{D}(s, s) = \mathbf{0}. \quad (12)$$

Here we write \mathbf{I} for the identity matrix and $\mathbf{0}$ for the zero matrix. We also write $\text{MVN}(\mathbf{m}, \mathbf{S})$ for the Multivariate Normal (Gaussian) distribution with mean \mathbf{m} , and variance matrix \mathbf{S} .

The above representation implies that by solving the initial value problems in (6), (11) and (12), and starting with an initial condition for $\boldsymbol{\xi}(s) = \boldsymbol{\xi}_0$ drawn from an arbitrary MVN distribution, one can easily derive the MVN probability distribution of $\boldsymbol{\xi}(t)$, for any time $t > s$. In this case, we say the LNA prediction for $\mathbf{X}(t)$ was initialised at time s . To simulate a path $\{\mathbf{X}(t) \mid t \geq 0\}$, we set $s = 0$. The process $\{\mathbf{X}(t) \mid t \geq 0\}$ modeled by the LNA is only an approximation of the true dynamics of the reaction network $\{\mathbf{Y}(t)/\Omega \mid t \geq 0\}$ where $\{\mathbf{Y}(t) \mid t \geq 0\}$ evolves according to (18) by the SSA. Therefore, when we refer to the notion of accuracy, we mean the accuracy in the distribution of $\mathbf{X}(t)$ when trying to capture the distribution of $\mathbf{Y}(t)/\Omega$ for each $t \geq 0$.

1.3.1 Accuracy of the LNA

The LNA accurately approximates the master equation in specific contexts. As discussed in SI (Section S2), the LNA is derived using the Central Limit Theorem, as Ω tends to ∞ , as an approximation of the probability distribution function satisfying the master equation. As a result, we expect the LNA to be accurate when Ω is sufficiently large. The value of Ω needed to ensure accuracy depends on the characteristics of the system's dynamics and the length of time interval where the approximation is sought.

If the LNA accurately represents the distribution of the state of a given system at some time-point s , it is expected to maintain this accuracy for a short time interval $[s, s + \delta)$ [61]. The duration for which the LNA remains accurate is influenced by the dynamics of the system and the level of stochasticity present. For instance, it was observed in [41] that for periodic systems with a moderate size Ω , the time interval over which the LNA retains its accuracy is approximately equal to the period of the system.

In situations where the system displays linear dynamics (i.e. the propensity functions in (2) are linear with respect to $\mathbf{Y}(t)$) the first two moments of the LNA coincide with those of solutions of the master equation [36]. Additionally, empirical studies comparing the distribution of the system at specific time-points, as predicted by the LNA, with histograms of the state distribution derived by simulated trajectories using the SSA, have shown agreement when the initial conditions are in the vicinity of stable equilibrium points (see e.g., [56, 41, 50]). Recent results identified the precise generic conditions under which the LNA is accurate near equilibrium points [22].

It is important to note that, for moderate system sizes, the LNA tends to fail in approximating the long-term dynamics of multi-stable and oscillatory systems [50, 5, 27, 56, 41].

1.3.2 Phase

Important in diagnosing this issue, and indeed the rest of this paper, is the idea of phase. For a given reaction network, we can qualitatively examine the dynamics of its paths and identify different stages of their evolution. For example, a phase could correspond to a specific species' peak or trough or intermediate point in the evolution of an oscillatory system or a point leading to one of the equilibria of a multi-stable system. For a stochastic path $\{\mathbf{X}(t) \mid t \geq 0\}$ and its deterministic path $\{\mathbf{x}(t) \mid t \geq 0\}$ we are able to isolate the points $\mathbf{X}(s)$ and $\mathbf{x}(s)$ at any time $s \geq 0$ on their path and qualitatively say what stages $\mathbf{X}(s)$ and $\mathbf{x}(s)$ are in with respect to the evolution of the entire path. We call these stages the phase of $\mathbf{X}(s)$ and $\mathbf{x}(s)$ respectively. Note that due to stochasticity, the phase of $\mathbf{X}(s)$ and the phase of $\mathbf{x}(s)$ can be different, particularly for large s . We also note that the consideration of phase is only useful for non-linear systems, since for linear systems, all trajectories lead to the same nearby equilibrium as $t \rightarrow \infty$ (or $t \rightarrow -\infty$). For networks with non-linear dynamics (e.g. oscillatory or multi-stable), once the LNA becomes inaccurate at some time-point τ , the phase of $\mathbf{X}(s)$, for $s \geq \tau$, becomes out of sync with the phase of $\mathbf{x}(s)$ causing $\boldsymbol{\xi}(s)$ to be too large for the LNA to make accurate predictions, even for short time transitions. That is, for times $s \geq \tau$, there will be no agreement between the LNA and SSA paths, at least for the next time interval. We call this phenomenon a phase drift. Therefore, initialising the LNA to the correct phase is a necessary condition for the LNA to be accurate. This leads us to speculate, if one can continually initialise the LNA with the correct phase so that the phase of $\mathbf{X}(s)$ is always that of the phase of $\mathbf{x}(s)$, and $\boldsymbol{\xi}(s)$ remains sufficiently small for all $s \geq 0$, then the LNA will remain accurate at all times and produce paths agreeing to those from the SSA. We argue that, for some classes of dynamical systems, this is indeed the case. For instance, it is shown in [41] that this is true for systems with RRE that has an attractive limit cycle solution and a range of moderate system sizes. We call this modelling technique the phase corrected Linear Noise Approximation (pcLNA).

1.4 The phase corrected Linear Noise Approximation (pcLNA)

Here we present the phase corrected Linear Noise Approximation algorithm in order to accurately simulate reaction networks with non-linear dynamics using LNA predictions. For each $t \geq 0$, we define the following ansatz;

$$\mathbf{X}(t) = G(\mathbf{X}(t)) + \Omega^{-1/2} \boldsymbol{\kappa}(t). \quad (13)$$

The map $G : \mathbb{R}^n \rightarrow \{\mathbf{x}(t) \mid t \geq 0\}$ takes the current stochastic state $\mathbf{X}(t)$ and maps it to a point $\mathbf{x}(s)$ on the deterministic evolution whose phase is the correct phase of $\mathbf{X}(t)$. Here the phase ‘‘correctness’’ depends on context. Then $\boldsymbol{\kappa}(t)$ denotes the perturbation of $\mathbf{X}(t)$ from $\mathbf{x}(s)$. We use this ansatz as follows.

That is, after each LNA step, the phase of the system is ‘‘corrected’’ such that $\mathbf{x}(s_i) = G(\mathbf{X}(t_i))$ and the fluctuations $\boldsymbol{\xi}(s_{i-1} + \Delta t)$ are replaced with the fluctuations remaining after the phase correction. Providing Δt is not too large, then any drifts in phase should be reset by this correction, ensuring the phase of deterministic state $\mathbf{x}(s_i)$ matches the phase of the stochastic state $\mathbf{X}(t_i)$. Hence for the next step of the algorithm, the LNA predictions are initialised using the time corresponding to this phase, preventing the increasing variance due to phase drifts. Indeed, $\{\boldsymbol{\kappa}(s_i) \mid i \in \mathbb{N}_0\}$ should have uniformly bounded variance and remain sufficiently small for the LNA predictions to be valid over the short time intervals $[s_i, s_i + \Delta t)$, $i \in \mathbb{N}_0$. Importantly for computational efficiency is that the same solutions of ODEs (6), (11) and (12) are used in all steps. The fact that these ODEs only need to be solved once before any simulations, rapidly increases the computation speed. The steps are illustrated in Figure 2 (A).

All that is preventing one from readily following the steps in the pcLNA algorithm is an explicit definition of the map G . A natural question to ask is, does there exist an explicit definition of the map G which will work for every reaction network? As we will soon see, the answer is no; phase is a concept specific to the dynamics of paths of reaction networks and so the map G is highly specific to the network.

Algorithm 1 General pcLNA algorithm

Inputs:

- a. Initial conditions: $s_0 = 0 = t_0$, $\mathbf{x}(0)$, $\mathbf{X}(0)$, Parameters: Δt , Ω .
- b. The system with RRE as in (6) and solution $\{\mathbf{x}(t) \mid t \geq 0\}$.
- c. The solutions \mathbf{C} and \mathbf{D} of (11), (12), respectively.
- d. Times $(t_i)_{i \in \mathbb{N}_0}$, with $t_i = t_0 + i\Delta t$.

Steps: Take $\boldsymbol{\kappa}(s_0) = \Omega^{1/2}(\mathbf{X}(0) - \mathbf{x}(0))$ and for $i = 1, 2, \dots$,

1. sample $\boldsymbol{\xi}(s_{i-1} + \Delta t)$ from the MVN distribution with mean $\mathbf{C}(s_{i-1}, s_{i-1} + \Delta t)\boldsymbol{\kappa}(s_{i-1})$, and variance matrix $\mathbf{D}(s_{i-1}, s_{i-1} + \Delta t)$;
2. compute $\mathbf{X}(t_i) = \mathbf{x}(s_{i-1} + \Delta t) + \Omega^{-1/2}\boldsymbol{\xi}(s_{i-1} + \Delta t)$;
3. set s_i such that $G(\mathbf{X}(t_i)) = \mathbf{x}(s_i)$ and set $\boldsymbol{\kappa}(s_i) = \Omega^{1/2}(\mathbf{X}(t_i) - \mathbf{x}(s_i))$.

Outputs: $\{\mathbf{X}(t_i) \mid i = 0, 1, 2, \dots\}$.

Despite this, we show, in Sections 1.5 and 1.6, the problem of finding G can be reduced since large classes of networks can be grouped together according to topological equivalence of their RRE solution $\{\mathbf{x}(t) \mid t \geq 0\}$ and simulated using the same explicit form of G .

1.5 Centre manifolds in n -dimensional reaction networks

In this section, we present some results from the theory of dynamical systems that are classical yet crucial for the development of our methods. We discuss how different dynamical systems can be grouped together based on the qualitative similarity of their behavior near their equilibrium points. Additionally, we explain how dynamical systems can be decomposed into linear and non-linear components in the vicinity of an equilibrium. This decomposition facilitates the computation and control of the system's phase, which is vital for the speed and accuracy of the pcLNA models.

First, suppose we have two ODE systems with velocities, \mathbf{F} and \mathbf{F}' , on \mathbb{R}^n and \mathbb{R}^m respectively. Also, suppose they each have an equilibrium point, \mathbf{x}_0 and \mathbf{x}'_0 , respectively. Then, near their equilibrium, the two dynamical systems are *locally topologically equivalent* if there exists a homeomorphism $\mathbf{h} : \mathbb{R}^n \rightarrow \mathbb{R}^m$ that is,

- (i) defined in a neighbourhood $A \subset \mathbb{R}^n$ of \mathbf{x}_0 ;
- (ii) satisfies $\mathbf{x}'_0 = \mathbf{h}(\mathbf{x}_0)$;
- (iii) maps paths of the system with velocity \mathbf{F} in the neighbourhood A onto paths of the system with velocity \mathbf{F}' in the neighbourhood $\mathbf{h}(A) \subset \mathbb{R}^m$, preserving the direction of time.

Intuitively, this means the paths of one dynamical system near its equilibrium can be continuously deformed onto paths of the other dynamical system near its equilibrium, and hence both systems exhibit paths that are qualitatively similar, i.e. have the same key features, near their equilibria.

Now we turn our focus to the deterministic evolution $\{\mathbf{x}(t) \mid t \geq 0\}$ solving the reaction rate equation (RRE) (6) when one parameter, say $\alpha \in \mathbb{R}$, is free to vary. We assume that the system has a non-hyperbolic equilibrium. That is, there exists an $\alpha_p \in \mathbb{R}$ such that,

$$\mathbf{F}(\mathbf{x}_p, \alpha_p) = \mathbf{0} \quad \text{and} \quad n_0 > 0, \tag{14}$$

where n_0, n_+, n_- denote the number of eigenvalues of the Jacobian matrix $\mathbf{J}(\mathbf{x}_p, \alpha_p)$ with zero, positive and negative real part, respectively. Following this, consider the extended system,

$$\begin{cases} \dot{\mathbf{x}} = \mathbf{F}(\mathbf{x}, \alpha), \\ \dot{\alpha} = 0. \end{cases} \quad (15)$$

Note that the Jacobian matrix of (15) evaluated at $\mathbf{x} = \mathbf{x}_p$ and $\alpha = \alpha_p$ is the $(n+1) \times (n+1)$ matrix,

$$\begin{pmatrix} 0 & 0 \\ \frac{\partial \mathbf{F}}{\partial \alpha} \Big|_{\substack{\mathbf{x}=\mathbf{x}_p \\ \alpha=\alpha_p}} & \mathbf{J}(\mathbf{x}_p, \alpha_p) \end{pmatrix}, \quad (16)$$

with $n_0 + 1$ eigenvalues with zero real part and $n - n_0$ eigenvalues with nonzero real part. Under the assumptions above, the following theorem holds (see [34, Theorem 5.1 and Lemma 5.1]).

Center Manifold Theorem *Let T^c be the eigenspace corresponding to the $n_0 + 1$ eigenvalues of (16) with zero real part. Then, there exists a smooth $(n_0 + 1)$ -dimensional manifold \mathcal{W}^c defined locally to $\mathbf{x} = \mathbf{x}_p$ and $\alpha = \alpha_p$ and tangent to T^c at $\mathbf{x} = \mathbf{x}_p$ and $\alpha = \alpha_p$.*

Moreover since $\dot{\alpha} = 0$ the hyperplanes, $\Pi_{\alpha'} = \{(\mathbf{x}, \alpha) \mid \alpha = \alpha'\}$, $\alpha' \in \mathbb{R}$ are invariant with respect to (15) and so, for each α local to α_p , \mathcal{W}^c is foliated by the n_0 dimensional manifolds $\mathcal{W}_\alpha^c = \mathcal{W}^c \cap \Pi_\alpha$. For each α local to α_p we call \mathcal{W}_α^c the centre manifold.

Finally, for each α local to α_p , there exists a neighbourhood $\Delta(\mathbf{x}_p)$ of $\mathbf{x} = \mathbf{x}_p$ such that if a path of (6) starting in $\Delta(\mathbf{x}_p)$, remains in $\Delta(\mathbf{x}_p)$, then this path approach \mathcal{W}_α^c as $t \rightarrow \infty$.

In other words, the Center Manifold Theorem states that there exists a parameter-dependent n_0 -dimensional invariant center manifold \mathcal{W}_α^c which is locally attracting. The next theorem (see [52]) describes a decomposition of non-hyperbolic systems into a linear and a non-linear component.

Shoshitaishvili Reduction Principle *Let α be local to α_p and let $(\mathbf{u}, \mathbf{v}, \mathbf{w})$ be a coordinate system with coordinates, $\mathbf{u} \in \mathbb{R}^{n_0}$, $\mathbf{v} \in \mathbb{R}^{n_-}$ and $\mathbf{w} \in \mathbb{R}^{n_+}$ lying on the eigenspaces corresponding to the n_0, n_+, n_- eigenvalues of $\mathbf{J}(\mathbf{x}_p, \alpha_p)$ with zero, positive and negative real part, respectively.*

Then, the centre manifold \mathcal{W}_α^c can be locally represented as a graph of a smooth function $\mathbf{V}_\alpha : \mathbb{R}^{n_0} \rightarrow \mathbb{R}^{n_- + n_+}$ with $\mathbf{V}_\alpha(\mathbf{u}) = O(\|\mathbf{u}\|^2)$;

$$\mathcal{W}_\alpha^c = \{(\mathbf{u}, \mathbf{v}, \mathbf{w}) \mid (\mathbf{v}, \mathbf{w}) = \mathbf{V}_\alpha(\mathbf{u})\}.$$

Moreover, near the equilibrium \mathbf{x}_p , (6) is locally topologically equivalent to the following system;

$$\begin{cases} \dot{\mathbf{u}} = \mathbf{A}\mathbf{u} + \mathbf{g}(\mathbf{u}, \mathbf{V}_\alpha(\mathbf{u})), \\ \dot{\mathbf{v}} = -\mathbf{v}, \\ \dot{\mathbf{w}} = \mathbf{w}, \end{cases} \quad (17)$$

near its equilibrium. Here \mathbf{A} is an $n_0 \times n_0$ matrix with all its eigenvalues, for $\alpha = \alpha_p$, on the imaginary axis and $\mathbf{g} : \mathbb{R}^{n_0} \rightarrow \mathbb{R}^{n_0}$ is a smooth function with Taylor expansions starting with at least quadratic terms.

The first equation in (17) is a restriction of equation (15) on the center manifold \mathcal{W}_α^c . The other two equations in (17) present linear, transient dynamics. Therefore, for small $|\alpha - \alpha_p|$, all non-transient events are captured on the invariant \mathcal{W}_α^c by the n_0 dimensional system of \mathbf{u} , where n_0 can be much smaller than n . It is worth noting that if $n_+ = 0$, the third equation vanishes, and the center manifold \mathcal{W}_α^c is attracting.

Furthermore, the last theorem states that there exists a parameter-dependent coordinate system on \mathcal{W}_α^c with coordinate \mathbf{u} , which satisfies the first equation in (17). Given the uniqueness of the eigenspace

²This implies that the Taylor expansion of $\mathbf{V}_\alpha(\mathbf{u})$ starts with at least quadratic terms.

of any matrix, particularly the Jacobian $\mathbf{J}(\mathbf{x}_p, \alpha_p)$, the coordinate $\mathbf{u} \in \mathbb{R}^{n_0}$ of \mathcal{W}_α^c indeed satisfies the first equation in (17). That is, the system described in (6) satisfying (14) is not only qualitatively similar to the system in (17) but also, when transformed into $(\mathbf{u}, \mathbf{v}, \mathbf{w})$ coordinates, it satisfies the first equation in (17) exactly.

1.6 Consequences on the pcLNA

Recall that we need to be able to define the map G to take a stochastic state \mathbf{X} and map it to a point on the deterministic evolution $\{\mathbf{x}(t) \mid t \geq 0\}$ with the correct phase of the stochastic state \mathbf{X} . Importantly, we have shown that if a reaction network has a RRE that contains a non-hyperbolic equilibrium, then one can perform a coordinate transformation from the standard basis in \mathbb{R}^n to the eigenbasis $(\mathbf{u}, \mathbf{v}, \mathbf{w})$ of $\mathbf{J}(\mathbf{x}_p, \alpha_p)$. Since local topological equivalence preserves the direction of time, then, assuming \mathbf{X} and $\{\mathbf{x}(t) \mid t \geq 0\}$ are close to \mathbf{x}_p , we could perform this coordinate transformation to transform \mathbf{X} and $\{\mathbf{x}(t) \mid t \geq 0\}$ into the eigenbasis and use their respective locations there in order to define G . In terms of the pcLNA, we know the dynamics in \mathbf{v} and \mathbf{w} are entirely linear and hence will be captured accurately by the LNA. Consequently, phase drifts, if they occur, will only take place in \mathbf{u} on the centre manifold \mathcal{W}_α^c . That is, letting $\{\mathbf{X}(t) = (\mathbf{U}(t), \mathbf{V}(t), \mathbf{W}(t)) \mid t \geq 0\}$ and $\{\mathbf{x}(t) = (\mathbf{u}(t), \mathbf{v}(t), \mathbf{w}(t)) \mid t \geq 0\}$ denote a stochastic path predicted by the LNA and the deterministic path respectively, the phase of $\mathbf{U}(s)$ will become out of sync with the phase of $\mathbf{u}(s)$ for large $s \geq 0$ whereas the phase of $(\mathbf{V}(s), \mathbf{W}(s))$ should match that of $(\mathbf{v}(s), \mathbf{w}(s))$. The stochastic perturbation $\boldsymbol{\xi}(s)$ will only grow too large in the dimension \mathbf{u} and not the others. Hence, when defining G , we only need phase corrections to keep $\boldsymbol{\xi}(s)$ small for each $s \geq 0$ in the reduced n_0 dimensions as opposed to n . The explicit definition of G will only depend on the position of the stochastic state in these n_0 dimensions; the same number of dimensions for all topologically equivalent networks. We make the following remark.

Remark *Equivalence classes made up of reaction networks with RREs containing a non-hyperbolic equilibrium and topologically equivalent solutions $\{\mathbf{x}(t) \mid t \geq 0\}$, have centre manifolds which share dimension n_0 as well as dynamics of paths on their respective manifolds.*

Hence, if one can define a phase correction map G which works for paths exhibiting such dynamics in the n_0 dimensions, then, in theory, this same map can be used to accurately simulate any reaction network in the equivalence class using the pcLNA algorithm.

2 Hopf bifurcation systems

2.1 The Hopf bifurcation

We now consider systems which present oscillatory behaviour. Let $\{\mathbf{X}(t) \mid t \geq 0\}$ be a reaction network in \mathbb{R}^n with deterministic evolution $\{\mathbf{x}(t) \mid t \geq 0\}$ solving the macroscopic reaction rate equation in (6). Suppose $\{\mathbf{x}(t) \mid t \geq 0\}$ depends smoothly on a parameter $\alpha \in \mathbb{R}$ and satisfies the conditions

- (H.I) there exists an $\alpha_p \in \mathbb{R}$ and $\mathbf{x}_p \in \mathbb{R}^n$ such that, $\mathbf{F}(\mathbf{x}_p, \alpha_p) = 0$,
- (H.II) when evaluated at $\mathbf{x} = \mathbf{x}_p$ and α local to α_p , the Jacobian of (6), has all negative eigenvalues except for a pair of complex conjugate eigenvalues $\lambda(\alpha)$, $\bar{\lambda}(\alpha)$ such that

$$\lambda(\alpha) = \mu(\alpha) + i\omega(\alpha), \quad \text{where} \quad \mu(\alpha_p) = 0, \quad \omega(\alpha_p) > 0.$$

Condition (H.I) is precisely the requirement for the macroscopic reaction rate equation to exhibit a equilibrium. Condition (H.II) ensures the equilibrium is non-hyperbolic and restricts all such networks

to consist of oscillatory paths. For any system satisfying the above conditions, we can define a phase correction map G .

Let (6) correspond to a reaction network in \mathbb{R}^n satisfying the conditions and α be local to α_p . Then, there exists a two dimensional centre manifold \mathcal{W}_α^c which is attracting and invariant for paths of (6).

Moreover, if (\mathbf{u}, \mathbf{v}) denote the coordinate system with coordinates, $\mathbf{u} \in \mathbb{R}^2$, $\mathbf{v} \in \mathbb{R}^{n-2}$ lying on the eigenspaces corresponding to the 2, $n-2$ eigenvalues of $\mathbf{J}(\mathbf{x}_p, \alpha_p)$ with zero, and negative real part, respectively. then, near the equilibrium \mathbf{x}_p , (6) is locally topologically equivalent to the dynamical system in (17). near its equilibrium. Here the matrix \mathbf{A} is an 2×2 matrix with all its eigenvalues, for $\alpha = \alpha_p$, on the imaginary axis, $\mathbf{g} : \mathbb{R}^n \rightarrow \mathbb{R}^2$.

Equation (17) tells us the non-linear dynamics, which the LNA fails to simulate accurately, lie on the centre manifold \mathcal{W}_α^c .

2.2 The pcLNA algorithm for Hopf bifurcation systems

Suppose we have a reaction network with macroscopic RRE as in (6) satisfying conditions (H.I), (H.II). Consider a stochastic trajectory $\{\mathbf{X}(t) \mid t \geq 0\}$ and a deterministic trajectory $\{\mathbf{x}(t) \mid t \in [0, T]\}$ of this network, for some value α of the bifurcation parameter that is near the critical α_p . Here $T \gg 0$ is the end of the time-interval where the solution of (6) is computed. We wish to define the phase map $G : \mathbb{R}^n \times [0, \infty) \rightarrow \{\mathbf{x}(t) \mid t \in [0, T]\}$, where $G(\mathbf{X}(t)) = \mathbf{x}(s)$, $s \in [0, T]$.

First, we find the \mathbf{u} coordinates in (17). We identify the conjugate pair of eigenvectors, $\mathbf{u}_1 \pm i\mathbf{u}_2$, corresponding to the complex eigenvalues of the Jacobian $\mathbf{J}(\mathbf{x}_p, \alpha)$ of the system in (6). The eigenspace corresponding to these complex eigenvalues is spanned by $\{\mathbf{u}_1, \mathbf{u}_2\}$, and while the vectors $\mathbf{u}_1, \mathbf{u}_2$ are not necessarily orthonormal, we can easily find an orthonormal basis $\{\hat{\mathbf{u}}_1, \hat{\mathbf{u}}_2\}$ of this eigenspace using Gram-Schmidt orthonormalisation or a similar method. Letting $\mathbf{R} = [\hat{\mathbf{u}}_1 \ \hat{\mathbf{u}}_2]$ the vector $\mathbf{U} = \mathbf{R}^\top(\mathbf{X} - \mathbf{x}_p) \in \mathbb{R}^2$ gives the \mathbf{u} -coordinates of the arbitrary state $\mathbf{X} \in \mathbb{R}^n$. Henceforth we write the map $G_3 : \mathbb{R}^n \rightarrow \mathbb{R}^2$, $\mathbf{U} = G_3(\mathbf{X}) = \mathbf{R}^\top(\mathbf{X} - \mathbf{x}_p)$ that performs this change of coordinates.

The trajectory $\{\mathbf{x}(t) \mid t \geq 0\}$ lies on its centre manifold (except initial transient periods), and $\mathbf{u}(t) = G_3(\mathbf{x}(t))$, $t \geq 0$, give its \mathbf{u} -coordinates on the centre manifold. As discussed in section 1.6, to control phase drifts we need to control the deviations of the stochastic trajectory in the \mathbf{u} coordinates. We therefore wish to minimise the distance of $\mathbf{U}(t) = G_3(\mathbf{X}(t))$ and $\mathbf{u}(t) = G_3(\mathbf{x}(t))$. We define the map $G_2 : \mathbb{R}^2 \in [0, T]$, where $s = G_2(\mathbf{U}) = \arg \min_{s' \in [0, T]} \|\mathbf{U} - \mathbf{u}(s')\|$, that gives the time minimising this distance. Finally, the map $G_1 : [0, T] \rightarrow \mathbb{R}^n$, $G_1(s) = \mathbf{x}(s)$ simply gives the state of $\{\mathbf{x}(t) \mid t \in [0, T]\}$ at time s . The phase correction map G is the convolution $G = G_1 \circ G_2 \circ G_3$, $\mathbf{x}(s) = G(\mathbf{X}) = G_1(G_2(G_3(\mathbf{X}))$ (see Figure 2B).

The perturbation $\boldsymbol{\kappa}(t) = \sqrt{\Omega}(\mathbf{X}(t) - G(\mathbf{X}(t)))$ has minimised \mathbf{u} coordinate. If the phase correction is performed in frequent times, the perturbations $\boldsymbol{\kappa}(t)$ will remain small.

Having defined the map G , we now provide the pcLNA algorithm for Hopf bifurcation systems in Algorithm 2.

3 Bi-stable systems

3.1 Bi-stability

We now consider systems that present bi-stability. We focus on the type of bi-stability arising in the systems presented in [2], [19] and [12].

Let $\{\mathbf{X}(t) \mid t \geq 0\}$ be a reaction network in \mathbb{R}^n with RRE limit (as $\Omega \rightarrow \infty$) satisfying (6) and Jacobian as in (7). There exist disjoint real subsets $\mathcal{A}_1, \mathcal{A}_2, \mathcal{A}_3$ of the space \mathcal{A} of the bifurcation parameter α such that

Algorithm 2 pcLNA for Hopf bifurcation systems

Inputs:

- a.. Initial conditions: $s_0 = 0 = t_0$, $\mathbf{x}(0)$, $\mathbf{X}(0)$, Parameters: Δt , Ω .
- b. System satisfying (H.I), (H.II), with solution $\{\mathbf{x}(t) \mid t \geq 0\}$ and orthonormal basis vectors, $\hat{\mathbf{u}}_1$, $\hat{\mathbf{u}}_2$, of the eigenspace corresponding to the conjugate pair of complex eigenvalues of $\mathbf{J}(\mathbf{x}_p, \alpha)$.
- c. The solutions \mathbf{C} and \mathbf{D} of (11), (12), respectively.
- d. Times $(t_i)_{i \in \mathbb{N}_0}$, with $t_i = t_0 + i\Delta t$.

Steps:

- A. Compute $\boldsymbol{\kappa}(s_0) = \Omega^{1/2}(\mathbf{X}(0) - \mathbf{x}(0))$.
- B. Set $\mathbf{R} = [\hat{\mathbf{u}}_1 \ \hat{\mathbf{u}}_2]$ and $\text{proj}_{\mathbf{R}} : \mathbb{R}^n \rightarrow \mathbb{R}^2$, $\mathbf{u} = \text{proj}_{\mathbf{R}}(\mathbf{x}) = \mathbf{R}^T(\mathbf{x} - \mathbf{x}_p)$. Compute $\{\mathbf{u}(t) = \text{proj}_{\mathbf{R}}(\mathbf{x}(t)) \mid t \geq 0\}$.
- C. For $i = 1, 2, \dots$,
 - 1. sample $\boldsymbol{\xi}(s_{i-1} + \Delta t)$ from the MVN distribution with mean $\mathbf{C}(s_{i-1}, s_{i-1} + \Delta t)\boldsymbol{\kappa}(s_{i-1})$, and variance matrix $\mathbf{D}(s_{i-1}, s_{i-1} + \Delta t)$;
 - 2. compute $\mathbf{X}(t_i) = \mathbf{x}(s_{i-1} + \Delta t) + \Omega^{-1/2}\boldsymbol{\xi}(s_{i-1} + \Delta t)$;
 - 3. compute $\mathbf{U} = \text{proj}_{\mathbf{R}}(\mathbf{X}(t_i))$ and set $s_i = \arg \min_s \|\mathbf{U} - \mathbf{u}(s)\|$ with $\|\cdot\|$ being the Euclidean norm, and $\boldsymbol{\kappa}(s_i) = \Omega^{1/2}(\mathbf{X}(t_i) - \mathbf{x}(s_i))$.

Outputs: $\{\mathbf{X}(t_i) \mid i = 0, 1, 2, \dots\}$.

- (B.I) for $\alpha \in \mathcal{A}_1$, (6) has a single fixed point $\mathbf{x} = \mathbf{x}_1^*$, and all eigenvalues of $\mathbf{J}(\mathbf{x}_1^*, \alpha)$ have negative real part.
- (B.II) for $\alpha \in \mathcal{A}_2$, (6) has two fixed points $\mathbf{x} = \mathbf{x}_1^*, \mathbf{x}_u$, and all eigenvalues of $\mathbf{J}(\mathbf{x}_1^*, \alpha)$ have negative real part, while all eigenvalues of $\mathbf{J}(\mathbf{x}_u, \alpha)$ have negative real part except one zero eigenvalue.
- (B.III) for $\alpha \in \mathcal{A}_3$, (6) has three fixed points $\mathbf{x} = \mathbf{x}_1^*, \mathbf{x}_u, \mathbf{x}_2^*$, and all eigenvalues of $\mathbf{J}(\mathbf{x}_i^*, \alpha)$, for $i = 1, 2$, have negative real part, while all eigenvalues of $\mathbf{J}(\mathbf{x}_u, \alpha)$ have negative real part except one real positive eigenvalue.

The system has three disjoint subsets of the parameter space, the first presenting a single, stable equilibrium, the second presenting a non-hyperbolic equilibrium and a stable equilibrium, while the third presents two stable equilibria and one unstable equilibrium. The Centre Manifold Theorem implies the existence of a locally defined (1+1)-dimensional manifold \mathcal{W}_α^c with an one-dimensional u coordinate system. For the case (B.III), the coordinate $\mathbf{u} \in \mathbb{R}$ lies on the direction of the eigenvector \mathbf{u} corresponding to the positive eigenvalue of $\mathbf{J}(\mathbf{x}_u, \alpha)$.

3.2 The pcLNA algorithm for bi-stable systems

Following the pcLNA principle, we construct a phase correction map G to control phase drifts for systems satisfying these conditions. As discussed in section 1.3.1, the LNA is long-time accurate if the conditions in (B.I) or (B.II) are satisfied. For the case where there is bi-stability as in (B.III), the standard LNA that uses a single deterministic solution to simulate a trajectory will produce trajectories centered around the “nearest” fixed point and therefore it will fail when there is a significant likelihood that a stochastic trajectory produced by SSA escapes from the nearest fixed point (see SI Figure S14). The main focus of phase correction is therefore to adapt the deterministic trajectory to allow for this event. At the very least, more than one deterministic trajectories will need to be used.

There is a simple way to predict the equilibrium that the current state is expected to converge. The u -coordinates of the two stable equilibria, $u_1^* = \mathbf{u}^T(\mathbf{x}_1^* - \mathbf{x}_u)$ and $u_2^* = \mathbf{u}^T(\mathbf{x}_2^* - \mathbf{x}_u)$, have different sign,

say $u_1^* < 0 < u_2^*$. Then, near \mathbf{x}_u , the eigenvector \mathbf{u} defines a separatrix, that is the trajectories with initial condition that has negative u -coordinate converge to \mathbf{x}_1^* , and vice versa.

The phase map $G(\mathbf{X})$ for a state \mathbf{X} of the stochastic trajectory is chosen to control perturbations in the u -coordinate. For this, it is essential that $G(\mathbf{X})$ and \mathbf{X} have u -coordinate of the same sign. To simplify notation, we write the map $\text{proj}_{\mathbf{u}} : \mathbb{R}^n \rightarrow \mathbb{R}$, $u = \text{proj}_{\mathbf{u}}(\mathbf{x})$. We consider a phase map that uses only two trajectories $\{\mathbf{x}_1(t) \mid t \geq 0\}$ and $\{\mathbf{x}_2(t) \mid t \geq 0\}$, the first converging to \mathbf{x}_1^* and the second to \mathbf{x}_2^* and their corresponding u -coordinates, $\{u_j(t) = \text{proj}_{\mathbf{u}}(\mathbf{x}_j(t)) \mid t \geq 0\}$ and $u_j^* = \text{proj}_{\mathbf{u}}(\mathbf{x}_j^*)$, $j = 1, 2$. Let $U = \text{proj}_{\mathbf{u}}(\mathbf{X})$. The phase map is then $G(\mathbf{X}) = \mathbf{x}_{j'}(s')$, where $j' \in \{1, 2\}$ such that $u_{j'}^* U > 0$ and $s' = \arg \min_s \|U - u_{j'}(s)\|$. That is, G maps \mathbf{X} to a point $\mathbf{x}_{j'}(s')$ where $j' \in \{1, 2\}$ is such that the point \mathbf{X} lies on the same side of the separatrix defined by u with the trajectory $\{\mathbf{x}_{j'}(t) \mid t \geq 0\}$ and s' such that $\mathbf{x}_{j'}(s')$ is the point on this trajectory that has the closest u -coordinate to the u -coordinate of \mathbf{X} . This phase map ensures that when the trajectory jumps from one side of the separatrix to the other, then the map also switches side. Using only two trajectories is the most minimal option; one may consider using more trajectories or using a new trajectory every time the state jumps to a different side of the separatrix, but this will be computationally more costly. In Algorithm 3, we describe the associated pcLNA simulation algorithm. In section 4, we show that this simple phase map is sufficient to achieve high levels of accuracy.

Algorithm 3 pcLNA for bistable systems

Inputs:

- a. Initial conditions: $s_0 = 0 = t_0$, $\mathbf{X}(0)$, $\mathbf{x}_j(0)$, $j = 1, 2$. Parameters: Δt , Ω .
- b. System satisfying (B.III) with eigenvector \mathbf{u} corresponding to the positive eigenvalue of $\mathbf{J}(\mathbf{x}_u, \alpha)$ and solutions $\{\mathbf{x}_j(t) \mid t \geq 0\}$ converging to \mathbf{x}_j^* , $j = 1, 2$, respectively.
- c. The solutions \mathbf{C} and \mathbf{D} of (11), (12), respectively.
- d. Times $(t_i)_{i \in \mathbb{N}_0}$, with $t_i = t_0 + i\Delta t$.

Steps:

- A. Define $\text{proj}_{\mathbf{u}} : \mathbb{R}^n \rightarrow \mathbb{R}$, $u = \text{proj}_{\mathbf{u}}(\mathbf{x}) = \mathbf{u}^T(\mathbf{x} - \mathbf{x}_u)$. Compute $\{u_j(t) = \text{proj}_{\mathbf{u}}(\mathbf{x}_j(t)) \mid t \geq 0\}$, and $u_j^* = \text{proj}_{\mathbf{u}}(\mathbf{x}_j^*)$, $j = 1, 2$.
- B. Compute $\boldsymbol{\kappa}(s_0) = \Omega^{1/2}(\mathbf{X}(0) - \mathbf{x}(0))$.
- C. For $i = 1, 2, \dots$,
 1. sample $\boldsymbol{\xi}(s_{i-1} + \Delta t)$ from the MVN distribution with mean $\mathbf{C}(s_{i-1}, s_{i-1} + \Delta t)\boldsymbol{\kappa}(s_{i-1})$, and variance matrix $\mathbf{D}(s_{i-1}, s_{i-1} + \Delta t)$;
 2. compute $\mathbf{X}(t_i) = \mathbf{x}(s_{i-1} + \Delta t) + \Omega^{-1/2}\boldsymbol{\xi}(s_{i-1} + \Delta t)$;
 3. compute $U = \text{proj}_{\mathbf{u}}(\mathbf{X}(t_i))$ and set $s_i = \arg \min_s \|U - u_{j'}(s)\|$ where $j' \in \{1, 2\}$ such that $u_{j'}^* U > 0$, and $\|\cdot\|$ being the Euclidean norm. Set $\boldsymbol{\kappa}(s_i) = \Omega^{1/2}(\mathbf{X}(t_i) - \mathbf{x}(s_i))$.

Outputs: $\{\mathbf{X}(t_i) \mid i = 0, 1, 2, \dots\}$.

4 Numerical investigations

As mentioned in Section 1.3, the LNA boasts fast computation of distributions of the stochastic process $\{\mathbf{X}(t) \mid t \geq 0\}$ as it only demands solving a set of ODEs to derive the RRE solution $\{\mathbf{x}(t) \mid t \geq 0\}$ in (6) and the drift and diffusion matrix solutions, \mathbf{C} and \mathbf{D} , of Eq. (11-12). Since the pcLNA algorithm also only requires such solutions, it also inherits its speed of simulation.

Next, we study the accuracy and computational efficiency of the pcLNA compared to the SSA. For this, we separately use SSA and pcLNA to produce a large number of long-time, stochastic trajectories

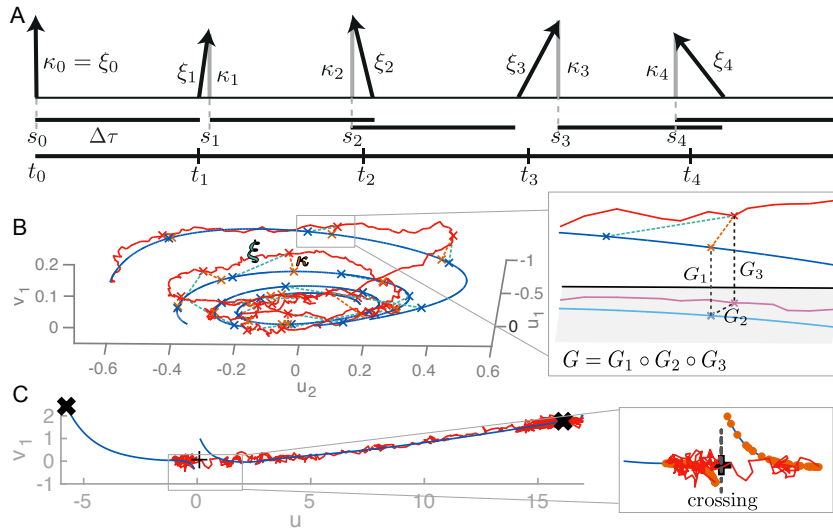


Figure 2: A. Phase Correction (PC) adjusts the times t_i to s_i and the perturbations $\xi(t_i)$ to $\kappa(s_i)$ between LNA steps. B-C. pLNA simulation trajectory (red) on (B) a Hopf Bifurcation system and (C) a bistable system (ode solution in blue). B. (Left) The points of PC (red crosses) and the perturbations before (ξ , light blue, dashed line) and after (κ , orange, dashed line) PC. (Right) Zoom in of a PC with the G map analysed to a convolution of G_j , $j = 1, 2, 3$. C. (Left) The two stable fixed points (x) and the unstable fixed point (+). (Right) Zoom in to the early part of simulation where a crossing was performed. G mappings shown (red circles on the ode solution).

and then compare their empirical probability distribution at various time-points. We perform this exercise for various systems, either presenting bi-stability or a Hopf bifurcation.

For Hopf bifurcation systems, we perform comparisons for all three qualitatively different cases where the system complex conjugate pair of eigenvalues in (H.II) has $\mu(\alpha) < 0, = 0, > 0$. In these three cases, the limiting RRE system presents quickly dampened oscillations, slowly dampened oscillations, and sustained oscillations, respectively (see also Figure 1A). For bistable systems, we focus on parameter values satisfying (B.III) (see Figure 1B, right) where the system present bistability, since in the case of (B.I), (B.II) the system is mono-stable and the standard LNA, under the usual conditions, is an accurate approximation (see 1.3.1).

The Hopf bifurcation systems used for comparisons are the following.

- The Brusselator system in [35], which is a classical oscillatory system involving complex interactions between two variables (for more details, see SI Section S3.2).
- The three-variable system in [63] that is the smallest reaction network presenting a Hopf bifurcation (see SI Section S3.3).
- The response of the NF- κ B signalling system to TNF α signals in [4], which is a system that involves 11 molecular populations involved in a large number of complex interactions (see SI Section S3.1).

For the first two systems above, we produced 1000 stochastic trajectories using SSA and pLNA for a time interval with length of 8τ , where τ the length of one period-cycle of the corresponding system. For the third system (where SSA simulations are substantially slower), we run 500 repetitions for a time-length of 4 periods of the system. We recorded the time taken to compute one stochastic trajectory for these time intervals, and then computed the median of these times, which we call CPU time in all the

presented figures. We also collected using these simulations the state, $(X_1(t_j), \dots, X_n(t_j))$ of all variables at various time-points, $t_j, j = 1, 2, \dots, J$ in each repetition, and computed the corresponding empirical density functions for the probability distribution of each variable $X_i(t_j)$ using kernel density estimation in MATLAB [25]. We present the results in Figure 3A and SI Figures S4- S12.

We clearly see that the pcLNA and SSA distributions are hardly distinguishable, while the CPU time is reduced by a magnitude of order $O(10) - O(10^3)$. The reduction in CPU time depends on the complexity of the system (number and speed of reactions) and the system size. Larger system sizes imply larger number of reaction occurrences and slower SSA simulations, while CPU times for pcLNA are not affected by system size.

The bi-stable systems considered are the following.

- The Genetic Toggle-Switch system in [12], which involves two-variables (for more details, see SI Section S3.4).
- The two-variable, simplified Cell-Cycle system presented in [2] (see SI Section S3.5).
- The Somitogenesis Switch system, presented in [19], that involves four variables and ten reactions (see SI Section S3.6).

We produced 1000 trajectories using SSA and pcLNA for the above systems, running for time intervals of length sufficient for convergence to one of the two stable fixed points by the solution of the corresponding RRE.

Note that if we initialise the system at a point close to one of the fixed points, then nearly all trajectories converge to that fixed point and the SSA simulations are well approximated by the standard LNA. Instead, we focused on simulations where the initial conditions are close to the unstable fixed point and where there is a substantial probability of convergence of a given trajectory to both fixed points. In this case, all the standard LNA trajectories will converge to the same fixed point and therefore can badly fail to approximate the SSA simulations (see SI Figure S14).

The pcLNA algorithm 3 requires the choice of at least two solutions of RRE that differ only by their initial condition and converge to a different fixed point. In the presented simulations, the two initial conditions are of the form $(1 - \epsilon) \mathbf{x}_u + \epsilon \mathbf{x}_j^* + \mathbf{c}, j = 1, 2$. Here $0 \leq \epsilon \leq 0.1$, \mathbf{x}_u the unstable fixed point and $\mathbf{x}_j^*, j = 1, 2$, the stable fixed points. The real vector \mathbf{c} performs a change of location in a direction orthogonal to the eigenvector corresponding to the real positive eigenvalue of the Jacobian $\mathbf{J}(\mathbf{x}^u)$. This change of location allows to view some short-time transient dynamics, but it is not necessary if one is interested in the long-time dynamics. For the specific initial conditions and other details, see SI Sections S3.4- S3.6.

The results are presented in Figure 3B and SI Figures S13, S15, S16. The two methods, SSA and pcLNA, are compared in the same way as the Hopf bifurcation system and the results are again showing the agreement between the two methods and similarly to above, significant reductions in the CPU time.

5 Discussion

The results in the previous section demonstrate the capability of the modified LNA method to effectively capture non-linear dynamics over long time intervals. The accuracy of the approximation combined with the analytical tractability of the LNA method establishes a robust framework for investigating reaction networks, and fitting these models to data. Fast and accurate simulations are critical for methods like Approximate Bayesian Computation [55, 40, 53, 57], in silico experimentation and sensitivity analysis [30, 23, 59, 47, 37, 51, 7, 44]. Furthermore, this work serves as a foundation for the development of methods that capitalize on the long-term accuracy and tractability of pcLNA, enabling the exact (under pcLNA) computation of the likelihood function of pcLNA and associated quantities, such as Fisher Information.

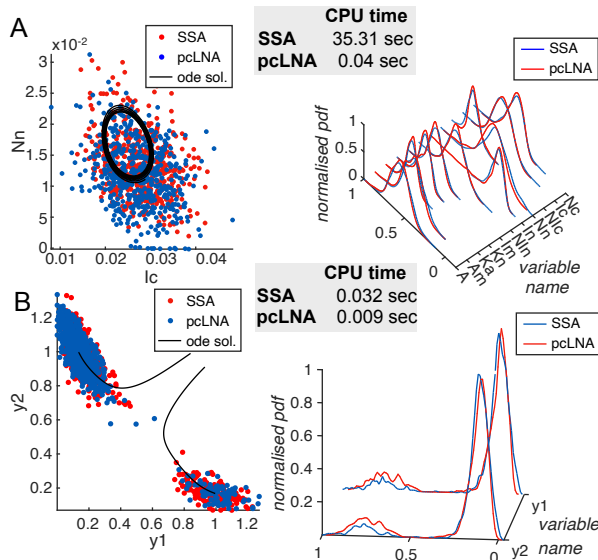


Figure 3: Comparison between SSA (red) and pcLNA (blue) for (A) the NF- κ B [4] and (B) the cell cycle [2] system. (Left) The states recorded after four cycles (A) and at $t = 100$ mins (B) of respectively $n = 500$ and $n = 1000$ simulations of the two systems and solutions of the corresponding RRE in (6). (Right) The corresponding empirical probability density functions of each of the system variables. The median CPU times for deriving one stochastic trajectory are also reported. See SI Section S3 for the details of the simulations.

We demonstrate the applicability of our technique across a variety of systems that exhibit two forms of non-linear behaviour, namely oscillations and bistability that are prevalent in biology and other fields. However, the modelling approach we propose, which draws on the centre manifold theory of dynamical systems, is applicable to a much broader range of reaction networks than those addressed in this paper. Indeed, for any network whose RRE solution contains a non-hyperbolic equilibrium, then providing one can produce a phase correction map G , the pcLNA algorithm can be used to simulate stochastic trajectories.

Supporting Information (SI)

The SI contains further mathematical details and numerical investigations referenced in this paper. We used PeTTSy [9] implemented in the MATLAB [25] environment and available at <https://wrap.warwick.ac.uk/id/eprint/77654/> to produce all results.

Supporting Information (SI)

S1 The stochastic simulation algorithm (SSA)

Consider paths of $\{\mathbf{Y}(t) \mid t \geq 0\}$ whose time-evolution is given by the random time change representation (RTC),

$$\mathbf{Y}(t) = \mathbf{Y}(0) + \sum_{j=1}^r \boldsymbol{\nu}_j N_j \left(\int_0^t \pi_j(\mathbf{Y}(s)) ds \right), \quad (18)$$

where, for $j \in \{1, \dots, r\}$, N_j are independent, unit Poisson processes corresponding to reaction R_j . To simulate such paths, the stochastic simulation algorithm (SSA) generates the next reaction at any given state. That is, if $\hat{\tau} > 0$ and $k \in \{1, 2, \dots, r\}$ correspond to the time to the next reaction and the index of the next reaction, respectively, it can be shown that, given the current state at time $t \geq 0$, $\mathbf{Y}(t) = \mathbf{y}$, the joint probability density function $p(\hat{\tau}, k \mid \mathbf{y}, t)$ of $\hat{\tau}$ and k are

$$p(\hat{\tau}, k \mid \mathbf{y}, t) = \pi_k(\mathbf{y}) \exp \left(- \sum_{j=1}^r \pi_j(\mathbf{y}) \tau \right). \quad (19)$$

where π_k the propensity function of reaction k . Informally, $p(\hat{\tau}, k \mid \mathbf{y}, t) d\tau$ represents the probability that, given that $\mathbf{Y}(t) = \mathbf{y}$, the next reaction in the system will occur at in the infinitesimal time interval $[t + \hat{\tau}, t + \hat{\tau} + d\hat{\tau})$ and will be a R_k reaction. Equation (19) implies that $\hat{\tau}$ is an exponential random variable with mean $1 / \sum_{j=1}^r \pi_j(\mathbf{y})$ and k is a statistically independent to τ integer random variable with point probabilities $\pi_k(\mathbf{y}) / \sum_{j=1}^r \pi_j(\mathbf{y})$. Hence we can sample such random variables exactly using the following; generate two random numbers, r_1 and r_2 , from the uniform distribution in the unit interval and take,

$$\hat{\tau} = - \frac{\log(r_1)}{\sum_{j=1}^r \pi_j(\mathbf{y})}, \quad (20)$$

and k to be the smallest integer such that,

$$\sum_{j=1}^k \pi_j(\mathbf{y}) > r_2 \sum_{j=1}^r \pi_j(\mathbf{y}). \quad (21)$$

Using the sampling procedure given by (20) and (21), we are able to construct the SSA for paths of $\{\mathbf{Y}(t) \mid t \geq 0\}$ which evolve exactly according to (18): Let $t_0 = 0$ and $\mathbf{Y}(t_0) = \mathbf{y}$. Then iteratively, for $i = 1, 2, \dots$,

1. generate two random numbers, r_1 and r_2 , from the uniform distribution on the unit interval;
2. sample $\hat{\tau}$ according to (20) and k according to (21);
3. set $t_i = t_{i-1} + \hat{\tau}$ and $\mathbf{Y}(t_i) = \mathbf{y} + \boldsymbol{\nu}_k$;
4. set $\mathbf{y} = \mathbf{Y}(t_i)$.

The result is the numerical simulation $\{\mathbf{Y}(t_i) \mid i \in \mathbb{N}_0\}$ where $(t_i)_{i \in \mathbb{N}_0}$ is a sequence of times, almost certainly not equally spaced. These paths are exact consequences of the chemical physics of stochastic reaction networks and hence capture the true dynamics of the network. For further details see [13, 14].

Consequently, one can compare distributions of states simulated by a model to that by the SSA in order to test the statistical accuracy of the model.

When performing the SSA simulations, we used the so-called *thinning* method to reduce the computational memory used. That is, we only record the SSA generated states at the first reaction times after times $m\delta t$, $m = 0, 1, 2, \dots, M$, for some large M and small δt . Furthermore, when we wish to compare SSA with pcLNA at specific times we use a smoothing spline interpolation to get the state of SSA (and similarly pcLNA) at specific time, say $t \in [(m-1)\delta t, m\delta t]$.

S2 The derivation of the Linear Noise Approximation (LNA)

To simplify notation, in this section we use the notation $x_t = x(t)$, for all states considered (i.e. \mathbf{x} , $\boldsymbol{\xi}$, \mathbf{X}). The LNA ansatz,

$$\mathbf{X}(t) = \mathbf{x}(t) + \Omega^{-1/2}\boldsymbol{\xi}(t), \quad (22)$$

implies that

$$\boldsymbol{\xi}_t = \sqrt{\Omega}(\mathbf{X}_t - \mathbf{x}_t)$$

and thus

$$\boldsymbol{\xi}_{t+dt} - \boldsymbol{\xi}_t = \sqrt{\Omega}((\mathbf{X}_{t+dt} - \mathbf{X}_t) - (\mathbf{x}_{t+dt} - \mathbf{x}_t)).$$

Using the form of RTC for \mathbf{X} and the RRE, we get that

$$\boldsymbol{\xi}_{t+dt} - \boldsymbol{\xi}_t = \sqrt{\Omega} \left(\sum_{j=1}^r \nu_j \{ \Omega^{-1} N_j (\Omega \rho_j(\mathbf{X}_t) dt) - \rho_j(\mathbf{x}_t) dt \} \right).$$

We next insert in the above sum the zero terms $0 = \rho_j(\mathbf{X}_t) dt - \rho_j(\mathbf{X}_t) dt$, where $\rho_j(\mathbf{X}_t) dt$ the mean of $\Omega^{-1} N_j (\Omega \rho_j(\mathbf{X}_t) dt)$, to get

$$\boldsymbol{\xi}_{t+dt} - \boldsymbol{\xi}_t = \sqrt{\Omega} \left(\sum_{j=1}^r \nu_j \{ \Omega^{-1} N_j (\Omega \rho_j(\mathbf{X}_t) dt) - \rho_j(\mathbf{X}_t) dt + (\rho_j(\mathbf{X}_t) - \rho_j(\mathbf{x}_t)) dt \} \right).$$

Then, by the Central Limit Theorem, as $\Omega \rightarrow \infty$,

$$Z = \frac{\Omega^{-1} N_j (\Omega \rho_j(\mathbf{X}_t) dt) - \rho_j(\mathbf{X}_t) dt}{\sqrt{\Omega^{-1} \rho_j(\mathbf{X}_t) dt}} \sim N(0, 1)$$

where $N(0, 1)$ is the standard normal distribution. Then for sufficiently large Ω ,

$$\sqrt{\Omega} (\Omega^{-1} N_j (\Omega \rho_j(\mathbf{X}_t) dt) - \rho_j(\mathbf{X}_t) dt) \approx Z \sqrt{\rho_j(\mathbf{x}_t) dt}. \quad (23)$$

Furthermore, by applying a Taylor expansion of $\rho_j(\mathbf{X}_t)$ about \mathbf{x}_t , we get

$$\sqrt{\Omega} (\rho_j(\mathbf{X}_t) - \rho_j(\mathbf{x}_t)) = \boldsymbol{\xi}(t)^T \nabla_{\mathbf{x}} \rho_j(\mathbf{x}_t) + O(\Omega^{-1/2}), \quad (24)$$

where $\nabla_{\mathbf{x}}^T = (\partial/\partial x_1, \dots, \partial/\partial x_n)$. Hence, for sufficiently large Ω ,

$$\boldsymbol{\xi}_{t+dt} - \boldsymbol{\xi}_t \approx \sum_j \nu_j \boldsymbol{\xi}(t)^T \nabla_{\mathbf{x}} \rho_j(\mathbf{x}_t) dt + \sum_j Z_j \nu_j \sqrt{\rho_j(\mathbf{x}_t) dt}$$

where Z_j are independent random variables following the standard normal distribution. Writing the above equation in matrix form, we get

$$d\xi = \mathbf{J}\xi dt + \mathbf{E} d\mathbf{B}_t, \quad (25)$$

where \mathbf{J} is the Jacobian matrix of the RRE, $\mathbf{E} = \mathbf{E}(\mathbf{x}) = \mathbf{S} \text{diag}(\sqrt{\rho_1(\mathbf{x})}, \dots, \sqrt{\rho_r(\mathbf{x})})$ the product of the stoichiometry matrix $\mathbf{S} = [\nu_1 \cdots \nu_r]$, and the square root of the diagonal matrix, with main diagonal entries $(\rho_1(\mathbf{x}), \dots, \rho_r(\mathbf{x}))$, and \mathbf{B}_t an n -dimensional Wiener process.

S3 Numerical Investigations

S3.1 The NF- κ B reaction network

The NF- κ B network consists of 11 species detailed in Table S1.

Table S1: Details of the 11 species characterising the NF- κ B network and their initial concentrations in three simulation settings with different value of the bifurcation parameter.

	Name	Description	Initial values Fig. S4	Initial values Fig. S5	Initial values Fig. S6
1	N_c	Free Cytoplasmic NFkB	0.0059	0.0065	0.0044
2	I_c	Free Cytoplasmic IkBa	0.0119	0.0289	0.0267
3	NI_c	Cytoplasmic NFkB-IkBa	0.0096	0.0611	0.0442
4	N_n	Free nuclear NFkB	0.0639	0.0111	0.0305
5	I_n	Free nuclear IkBa	0.0001	0.0010	0.0003
6	NI_n	Nuclear NFkB-IkBa	0.0002	0.0005	0.0005
7	I_m	IkBa transcription	0.0001	0.0002	0.0002
8	K_n	Kinase IKKn	0.0368	0.0071	0.0015
9	K_a	Kinase IKKa	0.0083	0.0034	0.0023
10	A_m	A20 transcription	0.0001	0.0001	0.0001
11	A	A20	0.0117	0.0139	0.0135

The ODE system for the NF- κ B system are given in table

The reaction rates used for the SSA are provided in the table below. The values of the parameters are the same as in Table S2 with suitable rate constant conversions applied.

Table S2: The parameters of NF- κ B system and the values used in simulations. Each of the three different levels of TNF α displayed in last row are used for the simulations in Figures S4,S5,S6, respectively.

parameter	description	value	unit
k_v	Cytoplasm:Nucleus ratio	3.3	–
k_p	IKK α production	0.0006	s^{-1}
k_a	Activation caused by TNF α	0.004	s^{-1}
k_i	Spontaneous IKK activation	0.003	s^{-1}
k_{a1a}	NF κ B-I κ B α association	0.5	$\mu M^{-1} s^{-1}$
k_{d1a}	NF κ B-I κ B α dissociation	0.0005	s^{-1}
k_{c1a}	Catalysis of IKK-I κ B α dimer	0.074	s^{-1}
k_{c2a}	Catalysis of IKK-I κ B α -NF κ B trimer	0.37	s^{-1}
k_{t2a}	degradation of I κ B α (IKK dependent from trimer)	0.1	s^{-1}
c_{4a}	Free I κ B α degradation	0.0005	s^{-1}
c_{5a}	NF κ B complexed I κ B α degradation	0.000022	s^{-1}
k_{i1}	NF κ B nuclear import	0.0026	s^{-1}
k_{e1}	NF κ B nuclear export	0.000052	s^{-1}
k_{e2a}	NF κ B-I κ B α nuclear export	0.01	s^{-1}
k_{i3a}	I κ B α nuclear import	0.00067	s^{-1}
k_{e3a}	I κ B α nuclear export	0.000335	s^{-1}
h	Order of hill function	2	–
k	Hill constant	0.0650	$\mu M/L$
c_{1a}	I κ B α mRNA synthesis	1.400e-07	$\mu M^{-1} s^{-1}$
c_{2a}	I κ B α translation rate	0.5	s^{-1}
c_{3a}	I κ B α mRNA degradation	0.0003	s^{-1}
c_1	I κ B α mRNA synthesis	1.4e-07	$\mu M^{-1} s^{-1}$
c_2	A20 mRNA translation	0.5	s^{-1}
c_3	A20 mRNA degradation	0.00048	s^{-1}
c_4	A20 degradation	0.0045	s^{-1}
k_{bA20}	Half-max A20 inhibition concentration	0.0018	$\mu M/L$
TNF- κ B	total NF- κ B concentration	0.08	μM
TIKK	total IKK concentration	0.08	μM
TNF α	Tumor necrosis factor alpha level	1.5 / 3.66 / 10	ng/mL

Table S3: The RRE ODE system equations for the NF- κ B system in [4]

\dot{N}_c	$= k_{d1a}NI_c - k_{a1a}N_cI_c - k_{i1}N_c + c_{5a}NI_c + k_vk_{e1}N_n + k_{t2a} \times (TNFKB - N_c - NI_c - N_n + NI_n)$
\dot{I}_c	$= k_{d1a}NI_c - k_{a1a}N_cI_c - k_{i3a}I_c + k_vk_{e3a}I_n - c_{4a}I_c + c_{2a}I_m - k_{c1a}K_aI_c$
\dot{NI}_c	$= k_{a1a}N_cI_c - k_{d1a}NI_c + k_vk_{e2a}NI_n - c_{5a}NI_c - k_{c2a}K_aNI_c$
\dot{N}_n	$= k_{d1a}NI_n - k_vk_{a1a}N_nI_n + k_{i1}N_c - k_vk_{e1}N_n$
\dot{I}_n	$= k_{d1a}NI_n - k_vk_{a1a}N_nI_n + k_{i3a}I_c - k_vk_{e3a}I_n - c_{4a}I_n$
\dot{NI}_n	$= k_vk_{a1a}NI_n - k_{d1a}NI_n - k_vk_{e2a}NI_n$
\dot{I}_m	$= c_{1a}(N_n^h/(N_n^h + (k/k_v)^h)) - c_{3a}I_m$
\dot{K}_n	$= k_p(TIKK - K_n - K_a)(k_{bA20}/(k_{bA20} + A \times TNF\alpha/10)) - k_aTNF\alpha K_n/10$
\dot{K}_a	$= k_aTNF\alpha K_n/10 - k_iK_a$
\dot{A}_m	$= c_1(N_n^h/(N_n^h + (k/k_v)^h)) - c_3A_m$
\dot{A}	$= c_2A_m - c_4A$

Table S4: The reactions and the corresponding propensity functions used for the SSA simulations of the NF- κ B system.

reaction	rate
$N_c + I_c \xrightarrow{k_{a1a}} NI_c$	$k_{a1a} \times I_c \times N_c/\Omega$
$NI_c \xrightarrow{k_{d1a}} N_c + I_c$	$k_{d1a} \times NI_c$
$N_n + I_n \xrightarrow{k_{a1a}} NI_n$	$k_vk_{a1a} \times I_n \times N_n/\Omega$
$NI_n \xrightarrow{k_{d1a}} N_n + I_n$	$k_{d1an} \times NI_n$
$K_a + I_c \xrightarrow{k_{c1a}} K_a + I_p$	$k_{c1a} \times K_a \times I_c/\Omega$
$K_a + NI_c \xrightarrow{k_{c2a}} K_a + NI_p$	$k_{c2a} \times K_a \times NI_c/\Omega$
$NI_p \xrightarrow{k_{t2a}} N_c$	$k_{t2a} \times NI_p$
$N_c \xrightarrow{k_{i1}} N_n$	$k_{i1} \times N_c$
$N_n \xrightarrow{k_{e1}} N_c$	$k_{e1} \times k_v \times N_n$
$NI_n \xrightarrow{k_{e2a}} NI_c$	$k_{e2a} \times k_v \times NI_n$
$I_c \xrightarrow{k_{i3a}} I_n$	$k_{i3a} \times I_c$
$I_n \xrightarrow{k_{e3a}} I_c$	$k_{e3a} \times k_v \times I_c$
$\emptyset \xrightarrow{H_I} I_m$	$(c_{1a}\Omega) \frac{N_n^h}{N_n^h + (k\Omega/k_v)^h}$
$I_m \xrightarrow{c_{2a}} I_m + I_c$	$c_{2a} \times I_m$
$I_m \xrightarrow{c_{3a}} \emptyset$	$c_{3a} \times I_m$
$I_c \xrightarrow{c_{4a}} \emptyset$	$c_{4a} \times I_c$
$I_n \xrightarrow{c_{4a}} \emptyset$	$c_{4a} \times I_n$
$NI_c \xrightarrow{c_{5a}} N_c$	$c_{5a} \times NI_c$
$\emptyset \xrightarrow{H_A} A_m$	$(c_1\Omega) \frac{N_n^h}{N_n^h + (k\Omega/k_v)^h}$
$A_m \xrightarrow{c_2} A_m + A$	$c_2 \times A_m$
$\vee A_m \xrightarrow{c_3} \emptyset$	$c_3 \times A_m$
$A \xrightarrow{c_4} \emptyset$	$c_4 \times A$
$K_i \xrightarrow{MA} K_n$	$k_p(TIKK - K_n - K_a) \frac{k_{bA20} \times \Omega}{(k_{bA20}\Omega) + A \times TNF\alpha/10}$
$K_n \xrightarrow{TNF\alpha/10 \times k_a} K_a$	$TNF\alpha/10 \times k_a \times K_n$
$K_a \xrightarrow{k_i} K_i$	$k_i \times K_a$

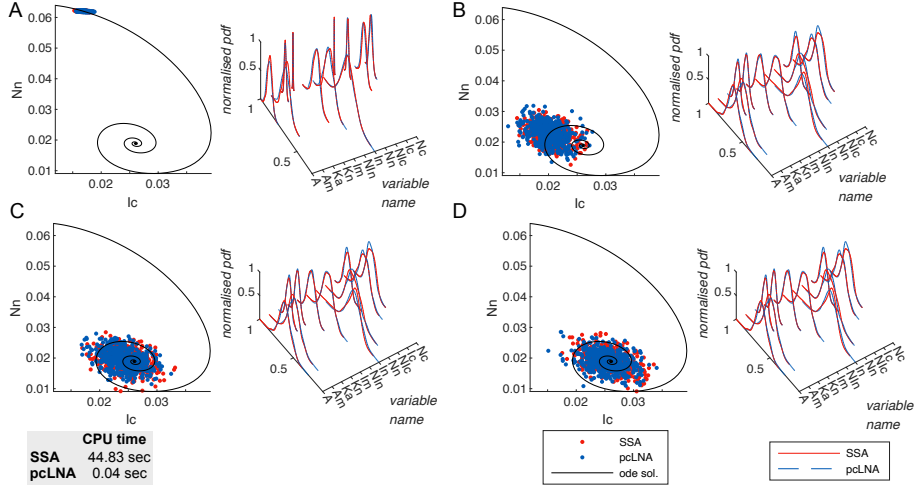


Figure S4: Comparison between SSA (red) and pcLNA (blue) for the NF- κ B system at $\Omega = 600,000$ with TNF α level = 1.5 ng/mL. Panels (A)–(D) correspond to times $t = 5, \tau + 5, 2\tau + 5, 3\tau + 5$, where $\tau \approx 102.095$ is the oscillation period. Each panel shows (left) the states recorded at time t of the simulations with solutions of the corresponding RRE, and (right) the corresponding empirical probability density functions of each system variable. Initial conditions and parameter values are given in Tables S1 and S2.

S3.1.1 Details for Figure 3

The bifurcation parameter of this system is the level of the Tumor necrosis factor alpha level (TNF α). The Hopf bifurcation value is $\approx 3.66 \text{ ng/mL}$. The simulations in Figure 3A are produced with the level of TNF α at the Hopf bifurcation value and with initial conditions given in Table S1 in the column “Initial values Fig. S5”.

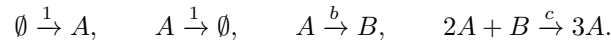
The empirical density functions of the probability distribution of each variable are derived using the kernel density function “ksdensity” in MATLAB [25]. To ensure good visibility of all the curves, we scale them. Specifically, both the x - and z -axis range from 0 to 1 since we divide both the value of each variable and their densities obtained for both SSA and pcLNA by their maximum observed values for both algorithms.

S3.1.2 Further numerical investigations for the NF- κ B system

See Figures S4, S5, S6.

S3.2 The Brusselator reaction network

The two dimensional Brusselator network, introduced in [35], consists of two chemical species, A and B , which undergo the following reactions,



If, for each $t \geq 0$, we let $\mathbf{Y}(t) = (Y_1(t), Y_2(t))^\top$ denote the number of molecules of A and B respectively, then these reactions occur according to the following intensities

$$\pi_1 = \Omega, \quad \pi_2 = Y_1, \quad \pi_3 = bY_1, \quad \pi_4 = cY_1^2Y_2/\Omega^2.$$

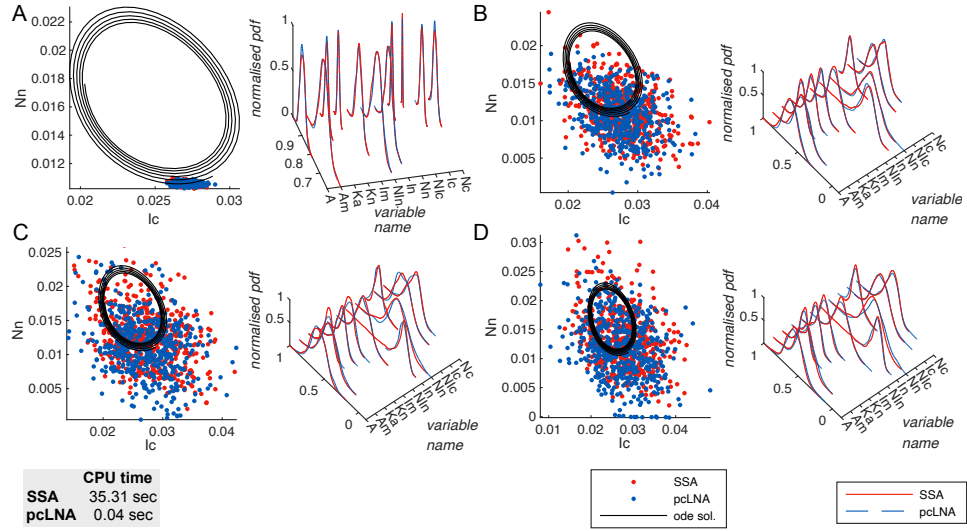


Figure S5: Comparison between SSA (red) and pcLNA (blue) for the NF- κ B system at $\Omega = 600,000$ with $\text{TNF}\alpha$ level = 3.66 ng/mL (Hopf bifurcation point). Panels (A)–(D) correspond to times $t = 5, \tau + 5, 2\tau + 5, 3\tau + 5$, where $\tau \approx 102.095$ is the oscillation period. Each panel shows (left) the states recorded at time t of the simulations with solutions of the corresponding RRE, and (right) the corresponding empirical probability density functions of each system variable. Initial conditions and parameter values are provided in Tables S1 and S2.

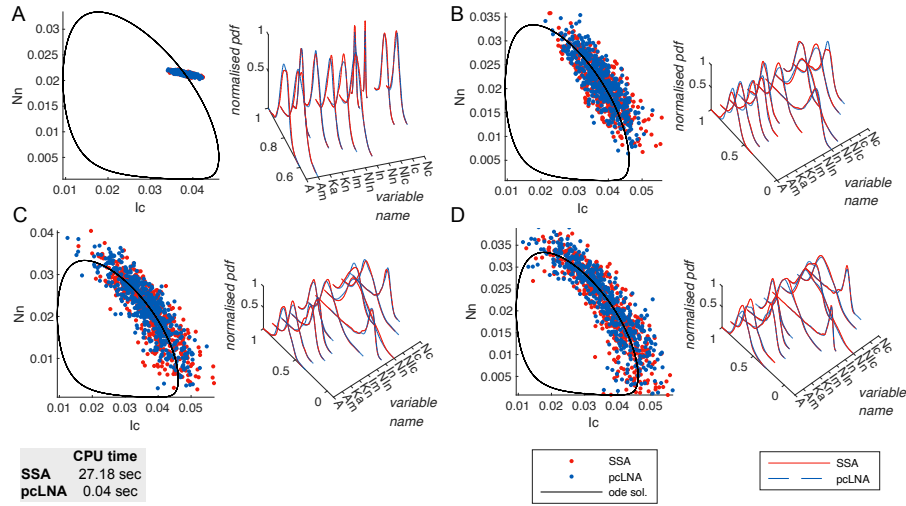


Figure S6: Comparison between SSA (red) and pcLNA (blue) for the NF- κ B system at $\Omega = 600,000$ with $\text{TNF}\alpha$ level = 10 ng/mL. Panels (A)–(D) correspond to times $t = 5, \tau + 5, 2\tau + 5, 3\tau + 5$, where $\tau \approx 102.095$ is the oscillation period. Each panel shows (left) the states recorded at time t of the simulations with solutions of the corresponding RRE, and (right) the corresponding empirical probability density functions of each system variable. Initial conditions and parameter values are listed in Tables S1 and S2.

With system size Ω and $\mathbf{X}(t) = \mathbf{Y}(t)/\Omega$ for each $t \geq 0$, the corresponding RRE solution in the $\Omega \rightarrow \infty$ limit is

$$\begin{cases} \dot{x}_1 = 1 - x_1(1 + b - cx_1x_2), \\ \dot{x}_2 = x_1(b - cx_1x_2). \end{cases} \quad (26)$$

From studying the Jacobian matrix of (26), we may conclude the system has a non-hyperbolic equilibrium at $(x_1, x_2) = (1, 2)^\top$, when $b = 2$ and $c = 1$, with purely imaginary conjugate eigenvalues $\pm i$. Through small deviations of b we deduce the Hopf bifurcation is supercritical with losses of stability occurring as the eigenvalues cross the imaginary axis. Parameters $b < 2$ give rise to a stable equilibrium, whereas $b > 2$ gives rise to an unstable equilibrium surrounded by a unique and stable limit cycle.

Table S5: Species in the Brusselator network and their initial concentrations for three different values of parameter b .

	Name	Description	Initial values Fig. S7	Initial values Fig. S8	Initial values Fig. S9
1	A	Chemical species A	0.8000	0.8000	1.0340
2	B	Chemical species B	1.5000	1.5000	2.9230

Table S6: Parameters used in the Brusselator network.

Parameter	Description	Value	Unit
c	Catalytic reaction rate	1	$\mu M^{-2} s^{-1}$
b	Conversion rate of A to B	1.7 / 2.0 / 2.3	s^{-1}

Table S7: The RRE ODEs for the mean-field dynamics of the Brusselator in the limit $\Omega \rightarrow \infty$.

$$\begin{cases} \dot{x}_1 = 1 - x_1(1 + b - cx_1x_2) \\ \dot{x}_2 = x_1(b - cx_1x_2) \end{cases}$$

Table S8: Reactions and their corresponding propensity functions for SSA simulations.

Reaction	Propensity function
$\emptyset \xrightarrow{1} A$	$\pi_1 = \Omega$
$A \xrightarrow{1} \emptyset$	$\pi_2 = Y_1$
$A \xrightarrow{b} B$	$\pi_3 = bY_1$
$2A + B \xrightarrow{c} 3A$	$\pi_4 = cY_1^2Y_2/\Omega^2$

S3.3 The smallest Hopf bifurcation reaction network

The system is described in [63].

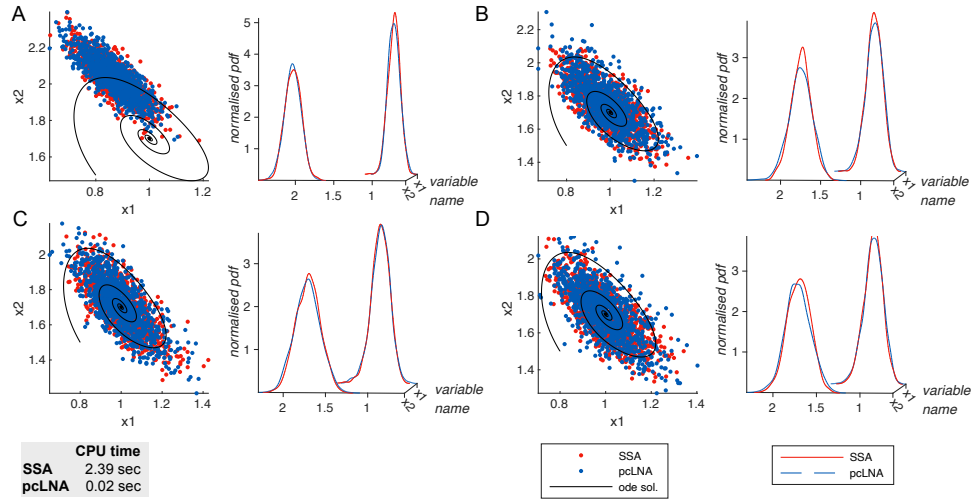


Figure S7: Comparison between SSA (red) and pcLNA (blue) for the Brusselator system at $\Omega = 1000$ with parameter $b = 1.7$. Panels (A)–(D) correspond to times $t = \tau + 0.5, 3\tau + 0.5, 5\tau + 0.5, 7\tau + 0.5$ with period $\tau = 6.2919$. Each panel shows (left) the states recorded at time t of the simulations with solutions of the corresponding RRE, and (right) the corresponding empirical probability density functions of each system variable. Initial conditions and parameter values are given in Tables S5 and S6.

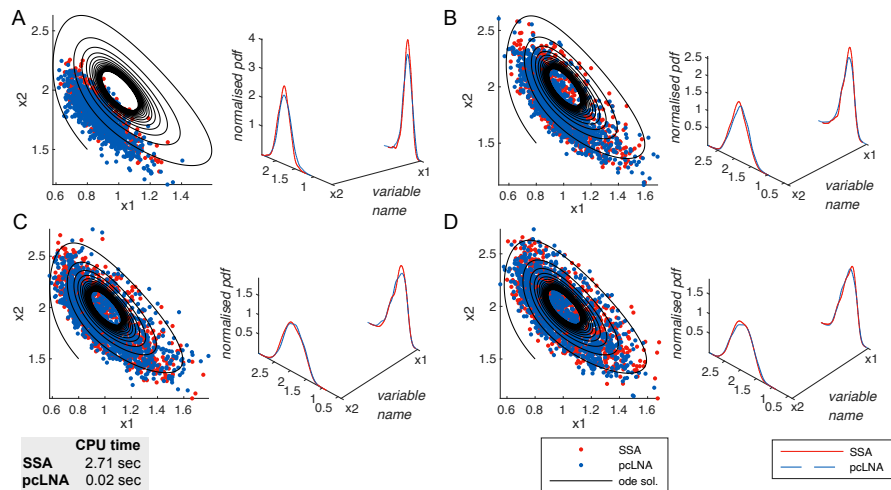


Figure S8: Comparison between SSA (red) and pcLNA (blue) for the Brusselator system at $\Omega = 1000$ with parameter $b = 2$. Panels (A)–(D) correspond to times $t = 0.5, 2\tau + 0.5, 4\tau + 0.5, 6\tau + 0.5$ with period $\tau = 6.35$. Each panel shows (left) the states recorded at time t of the simulations with solutions of the corresponding RRE, and (right) the corresponding empirical probability density functions of each system variable. Initial conditions and parameter values are provided in Tables S5 and S6.

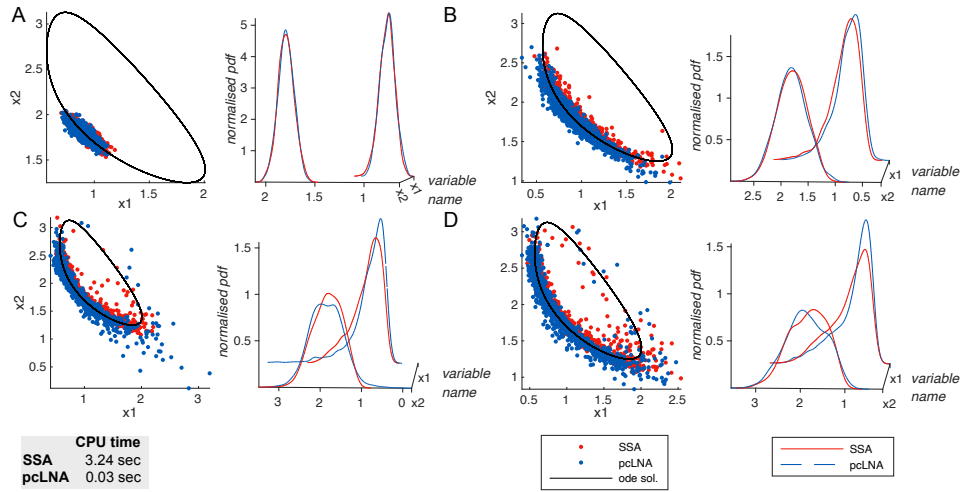


Figure S9: Comparison between SSA (red) and pcLNA (blue) for the Brusselator system at $\Omega = 1000$ with parameter $b = 2.3$. Panels (A)–(D) correspond to times $t = \tau + 0.5, 3\tau + 0.5, 5\tau + 0.5, 7\tau + 0.5$ with period $\tau = 6.4276$. Each panel shows (left) the states recorded at time t of the simulations with solutions of the corresponding RRE, and (right) the corresponding empirical probability density functions of each system variable. Initial conditions and parameter values are listed in Tables S5 and S6.

Table S9: Species in the smallest Hopf bifurcation network and their initial concentrations for three different values of parameter k_1 .

	Name	Description	Initial values Fig. S10	Initial values Fig. S11	Initial values Fig. S12
1	X_1	Species 1	3.8220	3.8220	2.4460
2	X_2	Species 2	3.8460	3.8460	1.0720
3	X_3	Species 3	5.1400	5.1400	1.2940

Table S10: Parameters used in the smallest Hopf bifurcation network.

Parameter	Description	Value	Unit
k_1	Activation rate	6 / 6.6 / 7	s^{-1}
k_2	Interaction rate between X_1 and X_2	2.2	s^{-1}
k_3	Degradation rate of X_2	2.2	s^{-1}
k_4	Conversion rate from X_1 to X_3	2.2	s^{-1}
k_5	Conversion rate from X_3 to X_2	2.2	s^{-1}
A	External activation strength	1	–

Table S11: The RRE ODEs for the mean-field dynamics of the smallest Hopf bifurcation network in the limit $\Omega \rightarrow \infty$.

$$\begin{aligned}
 \dot{x}_1 &= k_1 A x_1 - k_4 x_1 - k_2 x_1 x_2 \\
 \dot{x}_2 &= -k_3 x_2 + k_5 x_3 \\
 \dot{x}_3 &= k_4 x_1 - k_5 x_3
 \end{aligned}$$

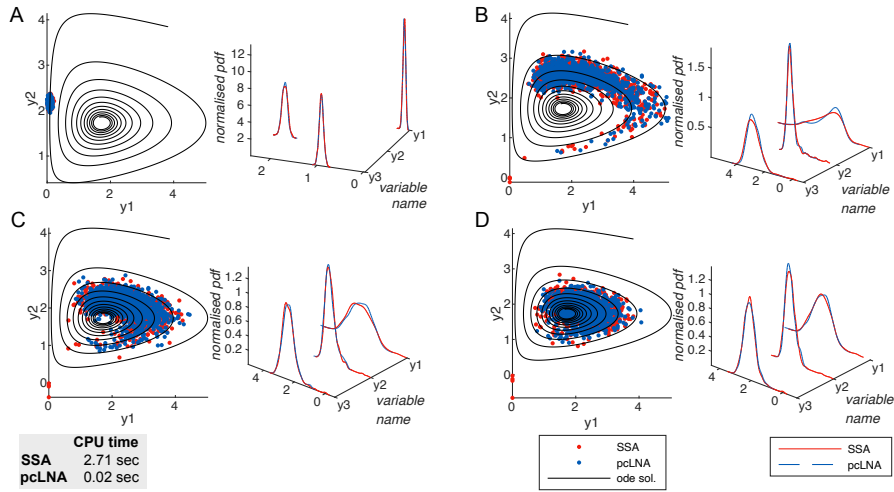


Figure S10: Comparison between SSA (red) and pcLNA (blue) for the smallest Hopf bifurcation network at $\Omega = 500$ with parameter $k_1 = 6$. Panels (A)–(D) correspond to times $t = \tau + 1, 3\tau + 1, 5\tau + 1, 7\tau + 1$ with period $\tau \approx 3$. Each panel shows (left) the states recorded at time t of the simulations with solutions of the corresponding RRE, and (right) the corresponding empirical probability density functions of each system variable. Initial conditions and parameter values are given in Tables S9 and S10.

Table S12: Reactions and their corresponding propensity functions for SSA simulations.

Reaction	Propensity function
$X_1 \xrightarrow{k_1 A} X_1$	$\pi_1 = k_1 A Y_1$
$X_1 + X_2 \xrightarrow{k_2} \emptyset$	$\pi_2 = k_2 \cdot Y_1 \cdot Y_2 / \Omega$
$X_2 \xrightarrow{k_3} \emptyset$	$\pi_3 = k_3 \cdot Y_2$
$X_1 \xrightarrow{k_4} X_3$	$\pi_4 = k_4 \cdot Y_1$
$X_3 \xrightarrow{k_5} X_2$	$\pi_5 = k_5 \cdot Y_3$

S3.4 The Genetic Toggle Switch reaction network

The system is described in [12].

Table S13: Species in the Genetic Toggle Switch network and their initial concentrations.

	Name	Description	Initial values ODE solution 1 Fig. S13	Initial values ODE solution 2 Fig. S13
1	x_1	Repressor 1	0.3067	0.4311
2	x_2	Repressor 2	0.4311	0.3067

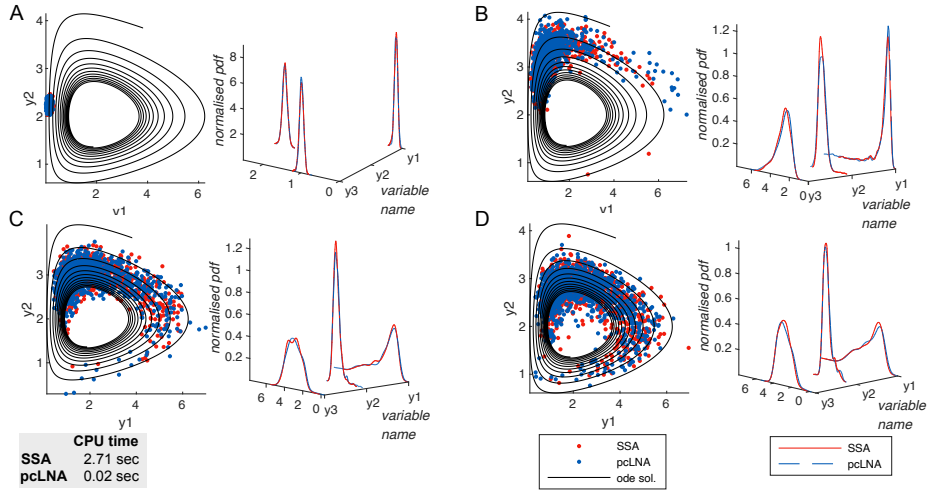


Figure S11: Comparison between SSA (red) and pcLNA (blue) for the smallest Hopf bifurcation network at $\Omega = 500$ with parameter $k_1 = 6.6$. Panels (A)–(D) correspond to times $t = \tau + 1, 3\tau + 1, 5\tau + 1, 7\tau + 1$ with period $\tau \approx 3$. Each panel shows (left) the states recorded at time t of the simulations with solutions of the corresponding RRE, and (right) the corresponding empirical probability density functions of each system variable. Initial conditions and parameter values are provided in Tables S9 and S10.

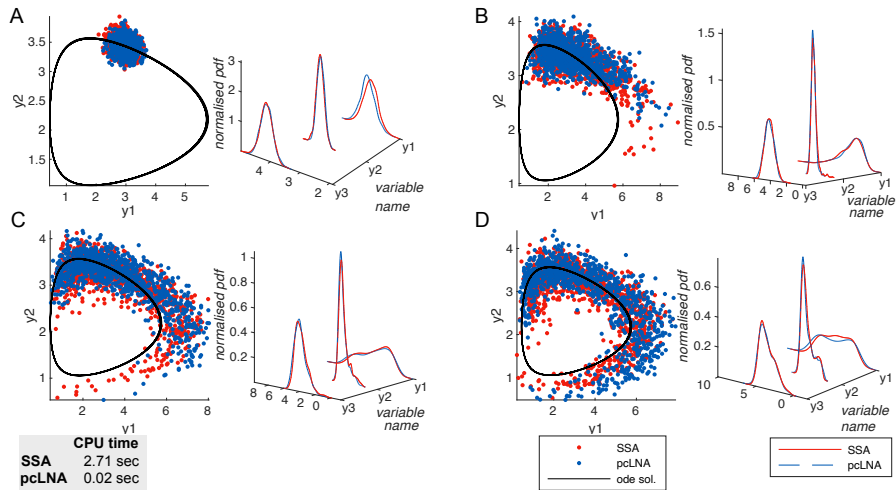


Figure S12: Comparison between SSA (red) and pcLNA (blue) for the smallest Hopf bifurcation network at $\Omega = 500$ with parameter $k_1 = 7$. Panels (A)–(D) correspond to times $t = \tau + 1, 3\tau + 1, 5\tau + 1, 7\tau + 1$ with period $\tau \approx 3$. Each panel shows (left) the states recorded at time t of the simulations with solutions of the corresponding RRE, and (right) the corresponding empirical probability density functions of each system variable. Initial conditions and parameter values are listed in Tables S9 and S10.

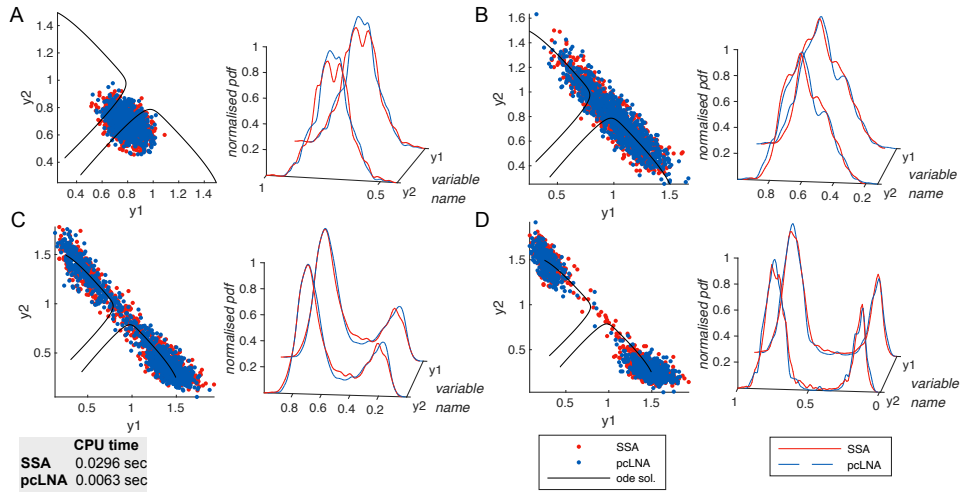


Figure S13: Comparison between SSA (red) and pcLNA (blue) for the Genetic Toggle Switch network at $\Omega = 100$. Panels (A)–(D) correspond to times $t = 0.5006, 2.0024, 5.0059, 9.5051$, respectively. Each panel shows (left) the states recorded at time t of the simulations with solutions of the corresponding RRE, and (right) the corresponding empirical probability density functions of each system variable. The initial conditions for the two ODE solutions are provided in Table S13, and the parameter values are given in Table S14.

Table S14: Parameters used in the Genetic Toggle Switch network.

Parameter	Description	Value	Unit
a_1	Activation rate of x_1	1.5	s^{-1}
a_2	Activation rate of x_2	1.5	s^{-1}
b	Hill coefficient for x_2 regulation of x_1	4	–
g	Hill coefficient for x_1 regulation of x_2	4	–
A	External activation strength	1	–

Table S15: The RRE ODEs for the mean-field dynamics of the Genetic Toggle Switch in the limit $\Omega \rightarrow \infty$.

$$\begin{cases} \dot{x}_1 = \frac{a_1 A}{1+x_2^b} - x_1 \\ \dot{x}_2 = \frac{a_2}{1+x_1^g} - x_2 \end{cases}$$

Table S16: Reactions and their corresponding propensity functions for SSA simulations.

Reaction	Propensity function
$X_1 \xrightarrow{a_1 A} X_1$	$\pi_1 = \frac{a_1 A \cdot \Omega}{1+Y_2^b}$
$X_1 \rightarrow \emptyset$	$\pi_2 = Y_1$
$X_2 \xrightarrow{a_2} X_2$	$\pi_3 = \frac{a_2 \cdot \Omega}{1+Y_1^g}$
$X_2 \rightarrow \emptyset$	$\pi_4 = Y_2$

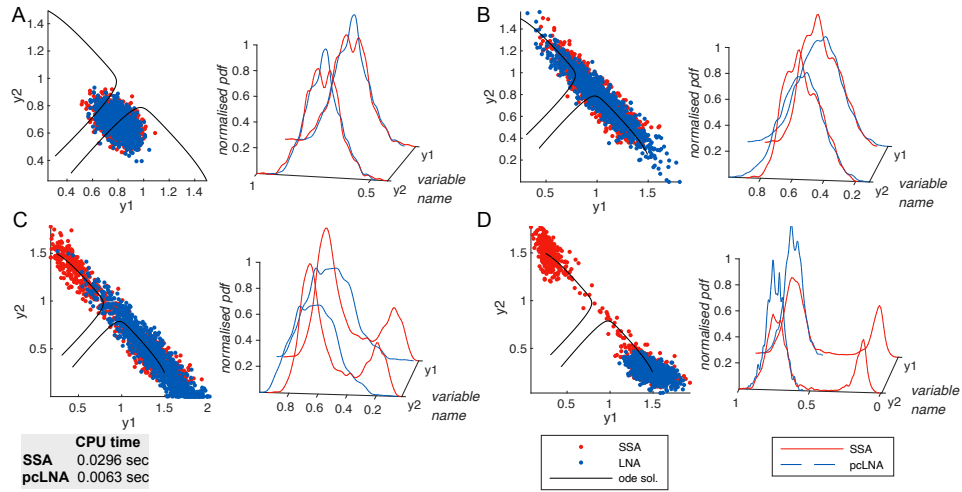


Figure S14: Comparison between SSA (red) and (standard) LNA (blue) for the Genetic Toggle Switch network at $\Omega = 100$. Panels (A)–(D) correspond to times $t = 0.5006, 2.0024, 5.0059, 9.5051$, respectively. Each panel shows (left) the states recorded at time t of the simulations with solutions of the corresponding RRE, and (right) the corresponding empirical probability density functions of each system variable. The initial conditions for the two ODE solutions are provided in Table S13, and the parameter values are given in Table S14.

S3.5 The Cell Cycle reaction network

The system is described in [2]; see section “A Two-Variable Example: The Cdc2-Cyclin B/Wee1 System”.

Table S17: Species in the Cell Cycle network and their initial concentrations.

	Name	Description	Initial values ODE solution 1 Fig. S15	Initial values ODE solution 2 Fig. S15
1	x_1	Cdc2-Cyclin B	0.9300	0.8400
2	y_1	Wee1	0.9100	0.9900

Table S18: Parameters used in the Cell Cycle network.

Parameter	Description	Value	Unit
a_1	Production rate of x_1	1	s^{-1}
a_2	Production rate of y_1	1	s^{-1}
b_1	Hill coefficient for y_1 regulation of x_1	200	–
b_2	Hill coefficient for x_1 regulation of y_1	10	–
γ_1	Hill exponent for y_1 regulation of x_1	4	–
γ_2	Hill exponent for x_1 regulation of y_1	4	–
K_1	Half-activation constant for x_1 regulation of y_1	2.3403	–
K_2	Half-activation constant for y_1 regulation of x_1	1	–
A	External activation strength	1	–

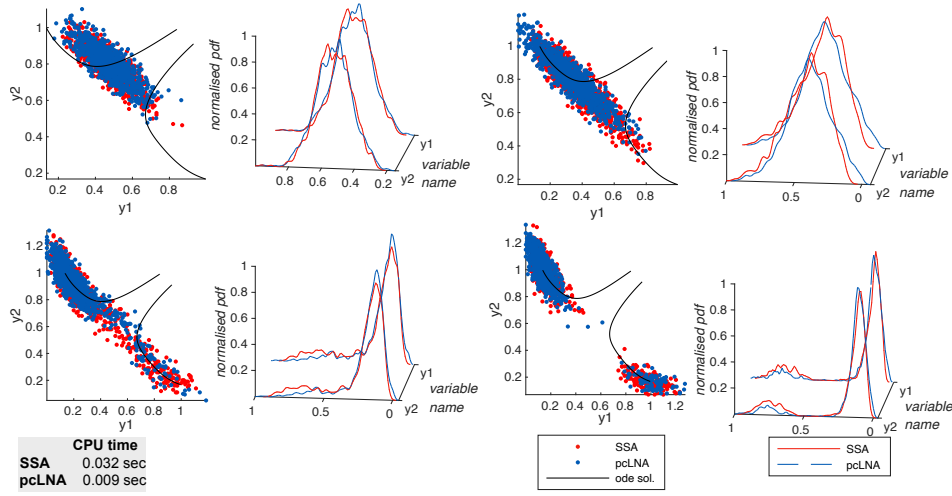


Figure S15: Comparison between SSA (red) and pcLNA (blue) for the Cell Cycle network at $\Omega = 100$. Panels (A)–(D) correspond to times $t = 0.5000, 9.9999, 49.9996, 100.0000$, respectively. Each panel shows (left) the states recorded at time t of the simulations with solutions of the corresponding RRE, and (right) the corresponding empirical probability density functions of each system variable. The initial conditions for the two ODE solutions are provided in Table S17, and the parameter values are given in Table S18.

Table S19: The RRE ODEs for the mean-field dynamics of the Cell Cycle system in the limit $\Omega \rightarrow \infty$.

$$\begin{cases} \dot{x}_1 &= a_1 - a_1 x_1 - \frac{b_1 x_1 ((A y_1)^{\gamma_1})}{K_1^{\gamma_1} + (A y_1)^{\gamma_1}} \\ \dot{y}_1 &= a_2 - a_2 y_1 - \frac{b_2 y_1 (x_1^{\gamma_2})}{K_2^{\gamma_2} + x_1^{\gamma_2}} \end{cases}$$

Table S20: Reactions and their corresponding propensity functions for SSA simulations.

Reaction	Propensity function
$X_1 \xrightarrow{a_1} X_1$	$\pi_1 = a_1 \cdot \Omega$
$X_1 \rightarrow \emptyset$	$\pi_2 = Y_1$
$X_2 \xrightarrow{b_1} X_2$	$\pi_3 = \frac{b_1 Y_1 ((A Y_2)^{\gamma_1})}{(K_1 \Omega)^{\gamma_1} + (A Y_2)^{\gamma_1}}$
$X_2 \rightarrow \emptyset$	$\pi_4 = Y_2$
$Y_1 \xrightarrow{a_2} Y_1$	$\pi_5 = a_2 \cdot \Omega$
$Y_1 \rightarrow \emptyset$	$\pi_6 = Y_2$
$Y_2 \xrightarrow{b_2} Y_2$	$\pi_7 = \frac{b_2 Y_2 ((Y_1)^{\gamma_2})}{(K_2 \Omega)^{\gamma_2} + (Y_1)^{\gamma_2}}$
$Y_2 \rightarrow \emptyset$	$\pi_8 = Y_3$

S3.6 The Somitogenesis Switch reaction network

The system is described in [19].

Table S21: Species in the Somitogenesis Switch network and their initial concentrations.

	Name	Description	Initial values ODE solution 1 Fig. S16	Initial values ODE solution 2 Fig. S16
1	R	Retinoic Acid (RA)	1.1500	1.2000
2	M_C	cyp26 mRNA	1.7467	1.7067
3	C	CYP26 protein	6.2333	6.0900
4	F	FGF8 protein	0.4933	0.4800

Table S22: Parameters used in the Somitogenesis Switch network.

Parameter	Description	Value	Unit
k_{s1}	RA synthesis rate via RALDH2	1	s^{-1}
RALDH2	RA synthetase concentration	7.1	–
k_{d1}	RA degradation via CYP26	1	s^{-1}
k_{d5}	Basal RA degradation	0	s^{-1}
V_0	Basal transcription of M_C	0.365	s^{-1}
V_{sc}	Activated transcription of M_C	7.1	s^{-1}
K_a	Activation constant for M_C production	0.5	–
n	Hill coefficient for FGF activation of M_C	2	–
k_{d3}	mRNA degradation rate	1	s^{-1}
k_{s2}	Translation rate of CYP26	1	s^{-1}
k_{d2}	CYP26 degradation rate	0.28	s^{-1}
k_{s3}	FGF8 synthesis rate	1	s^{-1}
M_0	Baseline activator level for FGF synthesis	5	–
K_I	Inhibition constant for RA effect on FGF	0.5	–
m	Hill coefficient for RA inhibition of FGF	2	–
k_{d4}	FGF degradation rate	1	s^{-1}
L	Normalization constant for spatial scaling	50	–
A	External activation strength	1	–

Table S23: The RRE ODEs for the mean-field dynamics of the Somitogenesis Switch in the limit $\Omega \rightarrow \infty$.

$$\begin{aligned}
\dot{R} &= k_{s1} \cdot \text{RALDH2} - k_{d1}RC - k_{d5}R \\
\dot{M}_C &= V_0 + \frac{V_{sc}F^n}{K_a^n + F^n} - k_{d3}M_C \\
\dot{C} &= k_{s2}M_C - k_{d2}C \\
\dot{F} &= k_{s3} \cdot \frac{M_0A/L \cdot K_I^m}{K_I^m + R^m} - k_{d4}F
\end{aligned}$$

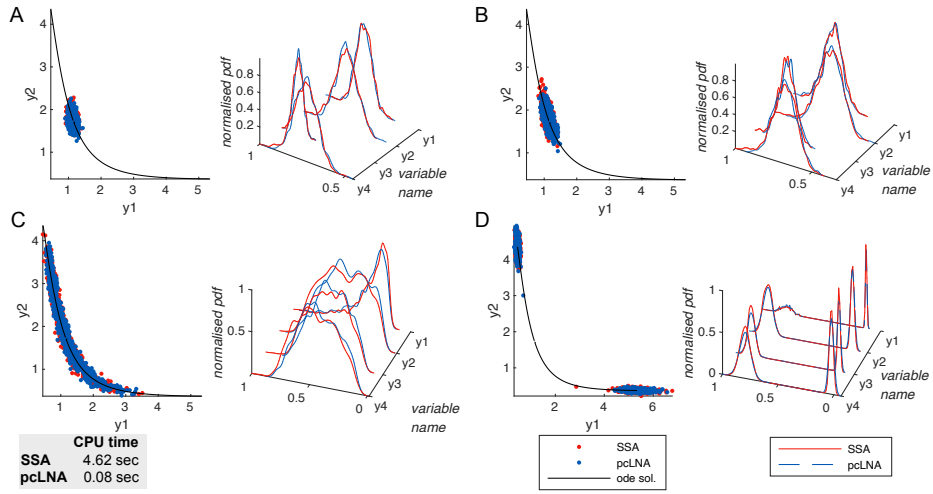


Figure S16: Comparison between SSA (red) and pcLNA (blue) for the Somitogenesis Switch network at $\Omega = 300$. Panels (A)–(D) correspond to times $t = 2, 5, 20, 99$, respectively. Each panel shows (left) the states recorded at time t of the simulations with solutions of the corresponding RRE, and (right) the corresponding empirical probability density functions of each system variable. The initial conditions for the two ODE solutions are provided in Table S21, and the parameter values are given in Table S22.

Table S24: Reactions and their corresponding propensity functions for SSA simulations.

Reaction	Propensity function
$R \xrightarrow{\text{syn}} R$	$\pi_1 = \Omega \cdot k_{s1} \cdot \text{RALDH2}$
$R + C \xrightarrow{\text{deg}} \emptyset$	$\pi_2 = \frac{k_{d1} RC}{\Omega}$
$R \xrightarrow{\text{deg}} \emptyset$	$\pi_3 = k_{d5} R$
$M_C \xrightarrow{\text{basal}} M_C$	$\pi_4 = \Omega \cdot V_0$
$M_C \xrightarrow{\text{FGF act}} M_C$	$\pi_5 = \frac{\Omega \cdot V_{sc} F^n}{(\Omega K_a)^n + F^n}$
$M_C \xrightarrow{\text{deg}} \emptyset$	$\pi_6 = k_{d3} M_C$
$C \xrightarrow{\text{trans}} C$	$\pi_7 = k_{s2} M_C$
$C \xrightarrow{\text{deg}} \emptyset$	$\pi_8 = k_{d2} C$
$F \xrightarrow{\text{syn}} F$	$\pi_9 = \frac{\Omega \cdot k_{s3} \cdot (M_0 A/L) \cdot (\Omega K_I)^m}{(\Omega K_I)^m + R^m}$
$F \xrightarrow{\text{deg}} \emptyset$	$\pi_{10} = k_{d4} F$

References

- [1] D.F. Anderson and T.G. Kurtz. *Continuous Time Markov Chain Models for Chemical Reaction Networks*, pages 3–42. Springer New York, 2011.
- [2] David Angeli, James E. Ferrell, and Eduardo D. Sontag. Detection of multistability, bifurcations, and hysteresis in a large class of biological positive-feedback systems. *Proceedings of the National Academy of Sciences*, 101:1822–1827, 2 2004.

- [3] Sol M. Fernández Arancibia, Hernán E. Grecco, and Luis G. Morelli. Effective description of bistability and irreversibility in apoptosis. *Phys. Rev. E*, 104:064410, Dec 2021.
- [4] L. Ashall, C.A. Horton, D.E. Nelson, P. Paszek, C.V. Harper, K. Sillitoe, S. Ryan, D.G. Spiller, J.F. Unitt, D.S. Broomhead, D.B. Kell, D.A. Rand, V. Sée, and M.R.H. White. Pulsatile stimulation determines timing and specificity of $\text{nf-}\kappa\text{b}$ -dependent transcription. *Science (American Association for the Advancement of Science)*, 324(5924):242–246, 2009.
- [5] R.P. Boland, T. Galla, and A.J. McKane. How limit cycles and quasi-cycles are related in systems with intrinsic noise. *Journal of Statistical Mechanics: Theory and Experiment*, 2008, 9 2008.
- [6] Zhixing Cao and Ramon Grima. Linear mapping approximation of gene regulatory networks with stochastic dynamics. *Nature Communications*, 9:3305, 8 2018.
- [7] Harsh Chhajer and Rahul Roy. Rationalised experiment design for parameter estimation with sensitivity clustering. *Scientific Reports*, 14:25864, 10 2024.
- [8] Francis Corson and Eric Dean Siggia. Geometry, epistasis, and developmental patterning. *Proceedings of the National Academy of Sciences*, 109:5568–5575, 4 2012.
- [9] Mirela Domijan, Paul E. Brown, Boris V. Shulgin, and David A. Rand. Pettsy: a computational tool for perturbation analysis of complex systems biology models. *BMC Bioinformatics*, 17:124, 3 2016.
- [10] Bärbel Finkenstädt, Dan J. Woodcock, Michal Komorowski, Claire V. Harper, Julian R. E. Davis, Mike R. H. White, David a. Rand, Barbel Finkenstadt, Dan J. Woodcock, Michal Komorowski, Claire V. Harper, Julian R. E. Davis, Mike R. H. White, and David a. Rand. Quantifying intrinsic and extrinsic noise in gene transcription using the linear noise approximation: An application to single cell data. *The Annals of Applied Statistics*, 7:1960–1982, 12 2013.
- [11] Sorana Froda and Sévérien Nkurunziza. Prediction of predator–prey populations modelled by perturbed odes. *Journal of Mathematical Biology*, 54(3):407–451, 2007.
- [12] Timothy S. Gardner, Charles R. Cantor, and James J. Collins. Construction of a genetic toggle switch in *escherichia coli*. *Nature*, 403:339–342, 1 2000.
- [13] D.T. Gillespie. A general method for numerically simulating the stochastic time evolution of coupled chemical reactions. *Journal of Computational Physics*, 22(4):403–434, 1976.
- [14] D.T. Gillespie. Exact stochastic simulation of coupled chemical reactions. *The Journal of Physical Chemistry*, 81(25):2340–2361, 1977.
- [15] D.T. Gillespie. A rigorous derivation of the chemical master equation. *Physica A*, 188(1):404–425, 1992.
- [16] D.T. Gillespie. The chemical Langevin equation. *The Journal of Chemical Physics*, 113(1):297–306, 07 2000.
- [17] D.T. Gillespie. Approximate accelerated stochastic simulation of chemically reacting systems. *The Journal of Chemical Physics*, 115(4):1716–1733, 07 2001.
- [18] D.T. Gillespie and L.R. Petzold. Improved leap-size selection for accelerated stochastic simulation. *The Journal of Chemical Physics*, 119(16):8229–8234, 10 2003.

- [19] Albert Goldbeter, Didier Gonze, and Olivier Pourquié. Sharp developmental thresholds defined through bistability by antagonistic gradients of retinoic acid and fgf signaling. *Developmental Dynamics*, 236:1495–1508, 6 2007.
- [20] Andrew Golightly, Laura E. Wadkin, Sam A. Whitaker, Andrew W. Baggaley, Nick G. Parker, and Theodore Kypraios. Accelerating bayesian inference for stochastic epidemic models using incidence data. *Statistics and Computing*, 33:134, 12 2023.
- [21] Didier Gonze, José Halloy, Jean-Christophe Leloup, and Albert Goldbeter. Stochastic models for circadian rhythms: effect of molecular noise on periodic and chaotic behaviour. *Comptes Rendus Biologies*, 326(2):189 – 203, 2003.
- [22] Theodore W. Grunberg and Domitilla Del Vecchio. A stein’s method approach to the linear noise approximation for stationary distributions of chemical reaction networks, 2024.
- [23] Ankit Gupta and Mustafa Khammash. An efficient and unbiased method for sensitivity analysis of stochastic reaction networks. *Journal of the Royal Society Interface*, 11:20140979–20140979, 2014.
- [24] A.V. Hill. The possible effects of the aggregation of the molecules of hæmoglobin on its dissociation curves. *The Journal of Physiology*, 40:i–vii, January 1910.
- [25] The MathWorks Inc. Matlab version: 9.13.0 (r2022b), 2023.
- [26] N. Ishii, K. Nakahigashi, T. Baba, M. Robert, T. Soga, A. Kanai, T. Hirasawa, M. Naba, K. Hirai, A. Hoque, P.Y. Ho, Y. Kakazu, K. Sugawara, S. Igarashi, S. Harada, T. Masuda, N. Sugiyama, T. Togashi, M. Hasegawa, Y. Takai, K. Yugi, K. Arakawa, N. Iwata, Y. Toya, Y. Nakayama, T. Nishioka, K. Shimizu, H. Mori, and M. Tomita. Multiple high-throughput analyses monitor the response of e. coli to perturbations. *Science (American Association for the Advancement of Science)*, 316(5824):593–597, 2007.
- [27] Y. Ito and K. Uchida. Formulas for intrinsic noise evaluation in oscillatory genetic networks. *Journal of Theoretical Biology*, 267:223–234, 11 2010.
- [28] Chen Jia and Ramon Grima. Holimap: an accurate and efficient method for solving stochastic gene network dynamics. *Nature Communications*, 15:6557, 8 2024.
- [29] K.A. Johnson and R.S. Goody. The original michaelis constant: Translation of the 1913 michaelis–menten paper. *Biochemistry (Easton)*, 50(39):8264–8269, 2011.
- [30] Michal Komorowski, Maria J Costa, David a Rand, and Michael P H Stumpf. Sensitivity, robustness, and identifiability in stochastic chemical kinetics models. *Proceedings of the National Academy of Sciences of the United States of America*, 108:8645–8650, 5 2011.
- [31] Michal Komorowski, Barbel Finkenstadt, Claire V Harper, David a Rand, Bärbel Finkenstädt, Claire V Harper, David a Rand, Barbel Finkenstadt, Claire V Harper, and David a Rand. Bayesian inference of biochemical kinetic parameters using the linear noise approximation. *BMC Bioinformatics*, 10:343, 10 2009.
- [32] T.G. Kurtz. Limit theorems for sequences of jump markov processes approximating ordinary differential processes. *Journal of Applied Probability*, 8(2):344–356, 1971.
- [33] T.G. Kurtz, Society for Industrial, and Applied Mathematics. *Approximation of Population Processes*. Number nos. 36-40 in Approximation of Population Processes. Society for Industrial and Applied Mathematics, 1981.

- [34] Y. Kuznetsov. *Elements of Applied Bifurcation Theory, 3rd Edic.* Society for Industrial and Applied Mathematics, 2011.
- [35] R. Lefever and G. Nicolis. Chemical instabilities and sustained oscillations. *Journal of Theoretical Biology*, 30(2):267–284, 1971.
- [36] Ioannis Lestas, Johan Paulsson, Nicholas E. Ross, and Glenn Vinnicombe. Noise in gene regulatory networks. *IEEE Transactions on Automatic Control*, 53:189–200, 1 2008.
- [37] Juliane Liepe, Paul Kirk, Sarah Filippi, Tina Toni, Chris P Barnes, and Michael P H Stumpf. A framework for parameter estimation and model selection from experimental data in systems biology using approximate bayesian computation. *Nature Protocols*, 9:439–456, 2 2014.
- [38] S. Mangan and U. Alon. Structure and function of the feed-forward loop network motif. *Proceedings of the National Academy of Sciences*, 100:11980–11985, 10 2003.
- [39] Elli Marinopoulou, Veronica Biga, Nitin Sabherwal, Anzy Miller, Jayni Desai, Antony D. Adamson, and Nancy Papalopulu. Hes1 protein oscillations are necessary for neural stem cells to exit from quiescence. *iScience*, 24:103198, 10 2021.
- [40] Paul Marjoram, John Molitor, Vincent Plagnol, and Simon Tavaré. Markov chain monte carlo without likelihoods. *Proceedings of the National Academy of Sciences*, 100:15324–15328, 12 2003.
- [41] G. Minas and D.A. Rand. Long-time analytic approximation of large stochastic oscillators: Simulation, analysis and inference. *PLoS Computational Biology*, 13, 7 2017.
- [42] G. Minas and D.A. Rand. Parameter sensitivity analysis for biochemical reaction networks. *Mathematical biosciences and engineering : MBE*, 16(5):3965–3987, 2019.
- [43] G. Minas, D.J. Woodcock, L. Ashall, C. Harper, M.R.H. White, and D.A. Rand. Multiplexing information flow through dynamic signalling systems. *PLoS computational biology*, 16(8):e1008076–e1008076, 2020.
- [44] Giorgos Minas and David A Rand. Parameter sensitivity analysis for biochemical reaction networks. *Mathematical Biosciences and Engineering*, 16:3965–3987, 4 2019.
- [45] Bela Novak and John J. Tyson. Numerical analysis of a comprehensive model of m-phase control in xenopus oocyte extracts and intact embryos. *Journal of Cell Science*, 106:1153–1168, 12 1993.
- [46] Joseph R. Pomerening, Sun Young Kim, and James E. Ferrell. Systems-level dissection of the cell-cycle oscillator: Bypassing positive feedback produces damped oscillations. *Cell*, 122:565–578, 8 2005.
- [47] Tom Rainforth, Adam Foster, Desi R. Ivanova, and Freddie Bickford Smith. Modern bayesian experimental design. *Statistical Science*, 39, 2 2024.
- [48] Nitzan Rosenfeld, Michael B Elowitz, and Uri Alon. Negative autoregulation speeds the response times of transcription networks. *Journal of Molecular Biology*, 323:785–793, 11 2002.
- [49] David Schnoerr, Guido Sanguinetti, and Ramon Grima. Approximation and inference methods for stochastic biochemical kinetics - a tutorial review. *Journal of Physics A: Mathematical and Theoretical*, 50, 8 2016.
- [50] M. Scott, B. Ingalls, and M. Kærn. Estimations of intrinsic and extrinsic noise in models of nonlinear genetic networks. *Chaos*, 16, 2006.

- [51] Ali Shahmohammadi and Kimberley B. McAuley. Using prior parameter knowledge in model-based design of experiments for pharmaceutical production. *AIChE Journal*, 66, 11 2020.
- [52] A. N. Shoshitaishvili. Bifurcations of topological type at singular points of parametrized vector fields. *Functional analysis and its applications*, 6(2):169–170, 1972.
- [53] S. A. Sisson, Y. Fan, and Mark M. Tanaka. Sequential monte carlo without likelihoods. *Proceedings of the National Academy of Sciences*, 104:1760–1765, 2 2007.
- [54] B. Swallow, D.A. Rand, and G. Minas. Bayesian inference for stochastic oscillatory systems using the phase-corrected linear noise approximation. *Bayesian Analysis*, pages 1 – 30, 2024.
- [55] Simon Tavaré, David J Balding, R C Griffiths, and Peter Donnelly. Inferring coalescence times from dna sequence data. *Genetics*, 145:505–518, 2 1997.
- [56] P. Thomas, H. Matuschek, and R. Grima. How reliable is the linear noise approximation of gene regulatory networks? *BMC Genomics*, 14, 2013.
- [57] Tina Toni, David Welch, Natalja Strelkowa, Andreas Ipsen, and Michael P.H Stumpf. Approximate bayesian computation scheme for parameter inference and model selection in dynamical systems. *Journal of The Royal Society Interface*, 6:187–202, 2 2009.
- [58] N.G. van Kampen. *Stochastic Processes in Physics and Chemistry*. Elsevier Science Publishers, Amsterdam, 1992.
- [59] Joep Vanlier, Christian A Tiemann, Peter AJ Hilbers, and Natal AW van Riel. Optimal experiment design for model selection in biochemical networks. *BMC Systems Biology*, 8:20, 2014.
- [60] P. Waage and C.M. Gulberg. Studies concerning affinity. *Journal of chemical education*, 63(12):1044–, 1986.
- [61] E.W.J. Wallace, D.T. Gillespie, K.R. Sanft, and L.R. Petzold. Linear noise approximation is valid over limited times for any chemical system that is sufficiently large. *IET Systems Biology*, 6:102–115, 8 2012.
- [62] Joshua S. Weitz, Sang Woo Park, Ceyhun Eksin, and Jonathan Dushoff. Awareness-driven behavior changes can shift the shape of epidemics away from peaks and toward plateaus, shoulders, and oscillations. *Proceedings of the National Academy of Sciences*, 117:32764–32771, 12 2020.
- [63] T. Wilhelm and R. Heinrich. Smallest chemical-reaction system with hopf-bifurcation. *J Math Chem*, 17:1–14, 1995.
- [64] Darren James Wilkinson. *Stochastic modelling for systems biology*, 2012.